PAPER

Stochastic dynamics driven by combined Lévy–Gaussian noise: fractional Fokker–Planck–Kolmogorov equation and solution

To cite this article: Wanrong Zan *et al* 2020 *J. Phys. A: Math. Theor.* **53** 385001

View the article online for updates and enhancements.

Recent citations

- Statistical solution to SDEs with α-stable Lévy noise via deep neural network
  Hao Zhang *et al*

IOP ebooks™

Bringing together innovative digital publishing with leading authors from the global scientific community.

Start exploring the collection−download the first chapter of every title for free.

Stochastic dynamics driven by combined Lévy–Gaussian noise: fractional Fokker–Planck–Kolmogorov equation and solution

Wanrong Zan[1], Yong Xu[1,2,8], Jürgen Kurths[3,4,5], Aleksei V Chechkin[6,7] and Ralf Metzler[6,8]

[1] Department of Applied Mathematics, Northwestern Polytechnical University, Xi'an 710072, People's Republic of China
[2] MIIT key Laboratory of Dynamics and Control of Complex Systems, Northwestern Polytechnical University, Xi'an 710072, People's Republic of China
[3] Potsdam Institute for Climate Impact Research, 14412 Potsdam, Germany
[4] Department of Physics, Humboldt University of Berlin, 12489 Berlin, Germany
[5] Saratov State University, 83, Astrakhanskaya Str., 410012 Saratov, Russia
[6] Institute for Physics and Astronomy, University of Potsdam, 14476 Potsdam, Germany
[7] Akhiezer Institute for Theoretical Physics National Science Center 'Kharkov Institute of Physics and Technology', 61108 Kharkov, Ukraine

E-mail: hsux3@nwpu.edu.cn and rmetzler@uni-potsdam.de

Abstract

Starting with a stochastic differential equation driven by combined Gaussian and Lévy noise terms we determine the associated fractional Fokker–Planck–Kolmogorov equation (FFPKE). For constant and power-law forms of an external potential we study the interplay of the two noise forms. Particular emphasis is paid on the discussion of sub- and superharmonic external potentials. We derive the probability density function solving the FFPKE and confirm the obtained shapes by numerical simulations. Particular emphasis is also paid to the stationary probability density function in the confining potentials and the question, to which extent the additional Gaussian noise effects changes on the probability density function compared to the pure Lévy noise case.

[8] Authors to whom any correspondence should be addressed.

(Some figures may appear in colour only in the online journal)

1. Introduction

The concept of random forces was introduced by Langevin *in lieu of* a more explicit, first-principle derivation of the apparent jittery motion of test particles in thermal environments where they are incessantly bombarded by neighbouring molecules [1]. Such fluctuations have become key statistical descriptors for many natural systems in physics, chemistry, biology, but also in economics etc. Systems in these fields are always affected by external or internal fluctuations, which are termed as 'noise'. These systems are then typically described by stochastic differential equations (SDEs). During the past years, interest in the study of these stochastic systems has increased significantly.

Gaussian white noise, the formal derivative of Brownian motion, is the earliest and most commonly adopted noise. There exist a vast literature on SDEs driven by Gaussian white noise. An important framework is the Fokker–Planck–Kolmogorov equation (FPKE), which governs the deterministic time evolution of the probability density functions (PDFs) corresponding to the SDE with Gaussian white noise [2]. However, analytical solutions of the FPKE are available only for some special cases. In other cases, solutions may be constructed by mapping the FPKE onto an imaginary time Schrödinger equation [3]. Concurrently, numerical methods are adopted for cases in which analytical solutions are difficult to obtain [4, 5].

Gaussian white noise stands out mathematically due to the universal convergence imposed by the central limit theorem on all independent, identically distributed (iid) random variables with finite variance. Practically, however, the Gaussian white noise is somewhat of an ideal realisation of random noise. Gaussian white noise is always used to describe small random fluctuations around a mean value, and it is no longer appropriate for systems exhibiting burst phenomena. In the latter cases Lévy noise often offers a better description. Lévy noise does not only consist of small perturbations but also of large jumps. In fact it was Mandelbrot who epitomised the role of Lévy noise as the driving noise for 'Lévy flights', random processes with long-tailed jump length distributions and fractal sample paths [6–10].

While Lévy flights can be described by SDEs driven by Lévy noise [11], a breakthrough was the formulation of the corresponding fractional FFPKEs [11–20]. These FFPKEs are similar in structure to the classical second-order FPKE, except for the fractional, αth-order of the highest derivative instead of the standard second-order [11–16]. The emergence of this fractional-order derivative makes the FFPKE difficult to solve, and there exist only several special cases that could be solved analytically [21–24]. Chechkin and coworkers specifically focussed on the non-stationary and stationary solutions of FFPKEs with different forms of an external, power-law potential of the form $U(x) \propto |x|^c/c$ [25–29]. Several exact results for Lévy flights in power potentials were obtained by Dubkov *et al* [30, 31]. In addition to analytical solutions, there are works adopted numerical methods to determine the PDF encoded by the FFPKEs [37, 62, 63]. Based on the solutions, Xu and coworkers studied the effect of Lévy noise to analyse bifurcation dynamics, stochastic resonance phenomena, first passage time and phase transitions [32–36, 38].

Due to the complexity of many real systems, there are situations which need to be addressed by a combination of more than one kind of noise. For example, in single gene expression there are both intrinsic noise and extrinsic noises [39–42]. Specifically, the random motion of a DNA-binding protein was shown to perform Lévy flights in the chemical co-ordinate on the DNA, but the protein may also normally-diffuse along the DNA, giving rise to an FFPKE with combined Gaussian and Lévy noises [43], compare also [44]. We also mention that the Earth's temperature was proposed to be modelled by a stochastic differential equation with a

combination of Gaussian and Lévy white noises [45]. The role of thermal and non-Gaussian noise on the dynamics of driven short overdamped Josephson junctions was studied in [46]. An alternative point of view for combining Lévy white noise with Gaussian white noise is that the latter represents a measurement noise or a diffusive drift in the setup analogous to the considerations in [47]. Such sampling noise could correspond to the diffusive drift, for instance, due to the local wind conditions, of a drone providing aerial footage of randomly searching animals employing Lévy search statistics [48–53] (see also references therein). In this context the question we want to answer is whether the presence of the additional Gaussian noise significantly alters the shape of the PDF, or whether the Lévy noise is tolerant to such a disturbance.

Duan and his coauthors [54] studied SDEs with Gaussian and Lévy noise. They investigated mean exit times and escape probabilities in terms of an FFPKE, which is derived in terms of an infinite series. Different from this approach, we here infer the FFPKE from the underlying SDE driven by combined Gaussian and Lévy noises via the respective characteristic functions. It is apparent that both fractional-order and second-order derivatives emerge in the FFPKE in the joint presence of Gaussian and Lévy noises [43] when the two noises contribute additively to the dynamics in the underlying SDE. Because of the co-existence of fractional-order and second-order derivatives, it becomes more difficult to obtain analytical solutions of FFPKEs. We will present analytical solutions wherever possible, combined with asymptotic behaviours and numerical solutions, in the force-free case and for different forms of external power-law potentials $U(x) \propto |x|^c/c$.

The remainder of this paper is organised as follows. In section 2, the SDE with Gaussian and Lévy noise and the corresponding FFPKE are introduced. In section 3, the FFPKE for constant external potential is solved and analysed. It is proved that the solution of the FFPKE possesses power-law tails. In section 4 the stationary analytical solutions for the FFPKE are derived for an harmonic external potential. In addition, the power-law asymptotic of the solution of the FFPKE is inferred. In section 5 the analysis for the quartic oscillator and strongly non-linear oscillator is studied, including an expansion of the analytical solution and the power-law tails. In section 6, the existence of the stationary state and the power-law asymptotic of the stationary PDF are proved. In the last section 7 we conclude this paper. Some additional information is provided in the appendix.

2. The model

In this section we introduce the model equations analysed in this paper. The starting SDE with Gaussian white noise and symmetric α-stable Lévy white noise is presented in section 2.1, and in section 2.2 the derivation of the associated FFPKE is described.

2.1. Starting stochastic differential equation with Gaussian and Lévy white noise terms

The starting SDE with Gaussian white noise and α-stable Lévy white noise reads

$$\frac{\mathrm{d}X}{\mathrm{d}t} = f(X) + \xi_\alpha(t) + \xi(t), \tag{1}$$

where $f(X) = -\mathrm{d}U(X)/\mathrm{d}X$, and $U(X)$ is the external potential. In the above, $\xi(t)$ is Gaussian white noise with zero mean, such that $\langle \xi(t) \rangle = 0$ and $\langle \xi(t)\xi(s) \rangle = 2D_\mathrm{G}\delta(t-s)$, where D_G is the intensity of the Gaussian white noise. Concurrently, $\xi_\alpha(t)$ is an external symmetric α-stable Lévy white noise, whose characteristic function is $Z(k) = \exp(-D_\mathrm{L}|k|^\alpha)$ (here and below, x is the variable in the real space and k stands for the Fourier space), where D_L and α ($0 < \alpha \leqslant 2$)

are the noise intensity and the stability index of the α-stable Lévy white noise, respectively. D_{L} and α satisfy the relationship $D_{\mathrm{L}} = \sigma^{\alpha}$, where σ is called the scale parameter. The symmetric α-stable Lévy white noise reduces to Gaussian white noise when $\alpha = 2$.

We denote $p(x, t|x_0, t_0)$, $Z_X(k, t - t_0|x_0, t_0)$ and $K_X(k, t - t_0|x_0, t_0)$ as the transition PDF, characteristic function, and cumulant generating function of the solution X of equation (1). The relationship among them is

$$\mathscr{F}[p(x, t|x_0, t_0)] = Z_X(k, t - t_0|x_0, t_0) = \exp(K_X(k, t - t_0|x_0, t_0))$$
$$= \mathbb{E}\left[\exp(ik[X(t) - X(t_0))|X(t_0) = x_0\right], \tag{2}$$

where k is the conjugate variable of $x - x_0$ (namely, $X(t) - X(t_0)$). Here $\mathscr{F}$ is the Fourier transformation defined as

$$\hat{f}(k) = \mathscr{F}[f] = \int_{-\infty}^{\infty} \mathrm{d}x \ \exp(ikx) f(x). \tag{3}$$

Similarly, for a given time lag $\delta t > 0$ we define the corresponding quantities for the increment processes, $\delta X(\delta t) = X(t + \delta t) - X(t)$ in the form

$$\mathscr{F}[p(x + \delta x, t + \delta t|x, t)] = \delta Z_X(k, \delta t|x, t) = \exp(\delta K_X(k, \delta t|x, t))$$
$$= \mathbb{E}[\exp(ik[X(t + \delta t) - X(t)])|X(t) = x], \tag{4}$$

where k is the conjugate variable of δx.

It is known that $\xi_\alpha(t)$ is the formal time derivative of the symmetric Lévy stable process $L_\alpha(t)$. The characteristic function about the increment δL of the process $L_\alpha(t)$ is $\delta Z_{\mathrm{L}}(k, \delta t) = \exp\left[-\delta t \times D_{\mathrm{L}}|k|^\alpha\right]$. Then we get the corresponding cumulant generating function $\delta K_{\mathrm{L}}(k, \delta t) = \delta t[-D_{\mathrm{L}}|k|^\alpha]$, according to equation (4). In addition, Gaussian white noise is the formal time derivative of Brownian motion $B(t)$, and the characteristic function for the increment δB is $\delta Z_B(k, \delta t) = \exp\left[-\delta t \times D_{\mathrm{G}}k^2\right]$. Thus, we can get the corresponding cumulant generating function $\delta K_B(k, \delta t) = \delta t[-D_{\mathrm{G}}k^2]$ through equation (4).

For the SDE (1) with a single noise type the corresponding FPKE is well known. For pure Gaussian noise the corresponding FPKE is the classical second-order FPKE [2]

$$\frac{\partial}{\partial t}p(x, t|x_0, t_0) = -\frac{\partial}{\partial x}\left(f(x)p(x, t|x_0, t_0)\right) + D_{\mathrm{G}}\frac{\partial^2}{\partial x^2}p(x, t|x_0, t_0). \tag{5}$$

Conversely, for the SDE with pure symmetric α-stable Lévy white noise the corresponding FFPKE reads [11, 14–16, 21, 24]

$$\frac{\partial}{\partial t}p(x, t|x_0, t_0) = -\frac{\partial}{\partial x}\left(f(x)p(x, t|x_0, t_0)\right) + D_{\mathrm{L}}\frac{\partial^\alpha}{\partial|x|^\alpha}p(x, t|x_0, t_0), \tag{6}$$

which is an FFPKE. Here the definition of the Riesz fractional derivative $\frac{\mathrm{d}^\alpha}{\mathrm{d}|x|^\alpha}$ is [25, 57, 58]

$$\frac{\mathrm{d}^\alpha f(x)}{\mathrm{d}|x|^\alpha} = \begin{cases} -\dfrac{D_+^\alpha f(x) + D_-^\alpha f(x)}{2 \ \cos(\pi\alpha/2)}, & \alpha \neq 1 \\ -\dfrac{\mathrm{d}}{\mathrm{d}x}Hf(x), & \alpha = 1 \end{cases}, \tag{7}$$

where

$$D_+^\alpha f(x) = \frac{1}{\Gamma(n-\alpha)} \frac{d^n}{dx^n} \int_{-\infty}^x \frac{f(\xi)}{(x-\xi)^{\alpha-n+1}} d\xi$$

$$D_-^\alpha f(x) = \frac{(-1)^n}{\Gamma(n-\alpha)} \frac{d^n}{dx^n} \int_x^\infty \frac{f(\xi)}{(\xi-x)^{\alpha-n+1}} d\xi \tag{8}$$

are the left and right Riemann–Liouville derivatives with $n = 1$ for $0 < \alpha < 1$, and $n = 2$ for $1 < \alpha \leqslant 2$. Besides, H is the Hilbert transformation operator

$$Hf(x) = \frac{1}{\pi} \fint_{-\infty}^{+\infty} \frac{f(\xi)}{x-\xi} d\xi. \tag{9}$$

Here $\fint$ is the integral in the principal value sense.

2.2. The fractional Fokker–Planck–Kolmogorov equation

We now show the derivation of the FFPKE corresponding to the SDE (1) with Gaussian and symmetric α-stable Lévy white noise. We will start from the Chapman–Kolmogorov–Smoluchowski equation for Markov processes,

$$p(x, t+\delta t|x_0, t_0) = \int_{-\infty}^\infty dy\, p(x, t+\delta t|y, t) p(y, t|x_0, t_0), \quad \forall \delta t > 0, \tag{10}$$

where $p(x, t+\delta t|x_0, t_0)$ and $p(y, t|x_0, t_0)$ are the PDF at time $t + \delta t$ and t, with the initial condition $X(t_0) = x_0$, respectively. Moreover $p(x, t+\delta t|y, t)$ is the transition PDF from $p(y, t|x_0, t_0)$ to $p(x, t+\delta t|x_0, t_0)$. Equation (10) can be rewritten in the equivalent form

$$p(x, t+\delta t|x_0, t_0) = \int_{-\infty}^{+\infty} dy \int_{-\infty}^{+\infty} \frac{dk}{2\pi} \exp\left(-ik(x-y) + \delta K_X(k, \delta t|y, t)\right) \times p(y, t|x_0, t_0), \tag{11}$$

where k is the conjugate variable of $x - y$. Letting $\delta t = 0$ in equation (11) the following equation holds,

$$p(x, t|x_0, t_0) = \int_{-\infty}^{+\infty} dy \int_{-\infty}^{+\infty} \frac{dk}{2\pi} \exp\left(-ik(x-y)\right) p(y, t|x_0, t_0). \tag{12}$$

Subtracting relation (12) from (11) produces

$$p(x, t+\delta t|x_0, t_0) - p(x, t|x_0, t_0) = \int_{-\infty}^{+\infty} dy \int_{-\infty}^{+\infty} \frac{dk}{2\pi} \exp\left(-ik(x-y)\right)$$
$$\times \left[\exp\left(\delta K_X(k, \delta t|y, t)\right) - 1\right] p(y, t|x_0, t_0), \tag{13}$$

where the $\delta K_X(k, \delta t|y, t)$ can be obtained using formula (4) and the SDE (1),

$$\delta K_X(k, \delta t|y, t) = ikf(y)\delta t - \delta t D_L |k|^\alpha - \delta t D_G k^2. \tag{14}$$

With this expression equation (13) can be rewritten, after expanding $\exp(\delta K_X(k, \delta t|y, t))$ in a Taylor series around δt,

$$p(x, t + \delta t|x_0, t_0) - p(x, t|x_0, t_0)$$

$$= \int_{-\infty}^{+\infty} \mathrm{d}y \int_{-\infty}^{+\infty} \frac{\mathrm{d}k}{2\pi} \exp\left(-\mathrm{i}k(x-y)\right) \left(\delta K_X(k, \delta t|y, t) + O(\delta t^2)\right) \times p(y, t|x_0, t_0)$$

$$= \int_{-\infty}^{+\infty} \mathrm{d}y \, \mathscr{F}^{-1}[\delta K_X(k, \delta t|y, t)] p(y, t|x_0, t_0) + O(\delta t^2), \tag{15}$$

where the term $\mathscr{F}^{-1}[\delta K_X(k, \delta t|y, t)]$ means the inverse Fourier transformation of $\delta K_X(k, \delta t|y, t)$ that can be calculated as

$$\mathscr{F}^{-1}[\delta K_X(k, \delta t|y, t)] = f(y)\delta t(-1)\delta'(x-y) - \delta t D_\mathrm{L}(-\Delta)^{\alpha/2}\delta(x-y)$$

$$- \delta t D_\mathrm{G}(-\Delta)\delta(x-y). \tag{16}$$

Inserting result (16) into (15) we get

$$p(x, t + \delta t|x_0, t_0) - p(x, t|x_0, t_0) = -\delta t \frac{\partial}{\partial x}\left(f(x)p(x, t|x_0, t_0)\right) + \delta t D_\mathrm{L}\frac{\partial^\alpha}{\partial|x|^\alpha}p(x, t|x_0, t_0)$$

$$+ \delta t D_\mathrm{G}\frac{\partial^2}{\partial x^2}p(x, t|x_0, t_0) + O(\delta t^2). \tag{17}$$

In the limit $\delta t \to 0$ we arrive at the FFPKE

$$\frac{\partial}{\partial t}p(x, t|x_0, t_0) = \lim_{\delta t \to 0}\frac{p(x, t + \delta t|x_0, t_0) - p(x, t|x_0, t_0)}{\delta t}$$

$$= -\frac{\partial}{\partial x}\left(f(x)p(x, t|x_0, t_0)\right) + D_\mathrm{L}\frac{\partial^\alpha}{\partial|x|^\alpha}p(x, t|x_0, t_0)$$

$$+ D_\mathrm{G}\frac{\partial^2}{\partial x^2}p(x, t|x_0, t_0). \tag{18}$$

Namely, for the SDE (1) with Gaussian and symmetric α-stable Lévy white noise, the corresponding fractional FPK equation is

$$\frac{\partial}{\partial t}p(x, t|x_0, t_0) = -\frac{\partial}{\partial x}\left(f(x)p(x, t|x_0, t_0)\right) + D_\mathrm{L}\frac{\partial^\alpha}{\partial|x|^\alpha}p(x, t|x_0, t_0)$$

$$+ D_\mathrm{G}\frac{\partial^2}{\partial x^2}p(x, t|x_0, t_0). \tag{19}$$

Equation (19) reduces to equation (5) when $D_\mathrm{L} = 0$ and to equation (6) when $D_\mathrm{G} = 0$. The FFPKE (19) can be directly inferred from the continuous time random walk theory with a combined jump length distribution [15, 43, 44, 59].

In the next section the FFPKE (19) with a constant potential $U(x) = \mathrm{const}$, a 'subharmonic' potential $U(x) = |x|^c$ with $0 < c < 2$, a harmonic potential $U(x) = x^2/2$, or a 'superharmonic' potential $U(x) = x^{2m+2}/(2m+2)$ with $m = 1, 2, \ldots$. will be studied. In our calculation the initial condition $p(x, t|x_0, t_0) = p(x, t|0, 0) = \delta(x)$ is considered. The symbol $p(x, t|0, 0)$ is replaced by the short-hand notation $p(x, t)$, which is the PDF at time t. We also introduce the symbol $Z_X(k, t)$ as the characteristic function corresponding to $p(x, t)$.

3. Fractional FPK equation with constant external potential

We start with analysing the FFPKE (19) for the zero-force case corresponding to a constant external potential. Analytical solutions are available for some special cases, and the power-law asymptotic of the solution is proved. Both solutions and power-law asymptotic are corroborated by numerical results.

3.1. Analytical solutions

For the FFPKE (19) with the external potential $U(x) = $ const the analytical solution in the Fourier space of this equation is derived. The analytical solutions in real space are obtained for the special cases $\alpha = 2$ and $\alpha = 1$.

The FFPKE (19) with $U(x) = $ const reads

$$\frac{\partial}{\partial t} p(x,t) = D_{\mathrm{L}} \frac{\partial^\alpha}{\partial |x|^\alpha} p(x,t) + D_{\mathrm{G}} \frac{\partial^2}{\partial x^2} p(x,t). \tag{20}$$

After applying the Fourier transformation (3), equation (20) turns into

$$\frac{\partial}{\partial t} Z_X(k,t) = -D_{\mathrm{L}} |k|^\alpha Z_X(k,t) - D_{\mathrm{G}} k^2 Z_X(k,t), \tag{21}$$

which has the solution

$$Z_X(k,t) = \exp\left(-\left(D_{\mathrm{L}} |k|^\alpha + D_{\mathrm{G}} k^2\right) t\right). \tag{22}$$

By the inverse Fourier transformation we get the PDF $p(x,t)$ in the real space. This transformation is not straightforward, and we can only implement it for the two special cases $\alpha = 2$ and $\alpha = 1$. [9]

For the special case $\alpha = 2$ the analytical solution (22) in Fourier space becomes $Z_X(k,t) = \exp(-(D_{\mathrm{L}} k^2 + D_{\mathrm{G}} k^2)t) = \exp(-(D_{\mathrm{L}} + D_{\mathrm{G}})k^2 t)$. The PDF $p(x,t)$ in real space can be obtained by the inverse Fourier transformation as the Gaussian

$$p(x,t)|_{\alpha=2} = \frac{1}{2\sqrt{(D_{\mathrm{L}} + D_{\mathrm{G}})\pi t}} \exp\left(-\frac{x^2}{4(D_{\mathrm{L}} + D_{\mathrm{G}})t}\right) \tag{23}$$

with the effective diffusivity $D_{\mathrm{L}} + D_{\mathrm{G}}$.

For the special case $\alpha = 1$ the analytical solution (22) becomes $Z_X(k,t) = \exp\left(-[D_{\mathrm{L}}|k| + D_{\mathrm{G}} k^2]t\right)$. The corresponding PDF $p(x,t)$ in the real space yields from the inverse Fourier transformation,

$$p(x,t)|_{\alpha=1} = \frac{1}{4\sqrt{D_{\mathrm{G}} \pi t}} \left[\exp\left(\frac{(D_{\mathrm{L}} t + ix)^2}{4 D_{\mathrm{G}} t}\right) \mathrm{erfc}\left(\frac{D_{\mathrm{L}} t + ix}{2\sqrt{D_{\mathrm{G}} t}}\right) + \mathrm{c.c}\right], \tag{24}$$

where c.c is the complex conjugate of the first part in the curly brackets on the right hand side of relation (24), and the function $\mathrm{erfc}(x)$ is the complementary error function. Two special examples are worthwhile considering:

---

[9] Note that the inverse Fourier transform for arbitrary Lévy stable density can be achieved in terms of Fox H-functions [15, 64, 65].

(A) If only Gaussian noise exists, that is, $D_L = 0$, relation (24) reduces to the Gaussian distribution

$$p(x,t)|_{\alpha=1} = \frac{1}{2\sqrt{D_G \pi t}} \exp\left(-\frac{x^2}{4D_G t}\right), \quad D_L = 0. \tag{25}$$

Although the symbol $p(x,t)|_{\alpha=1}$ continues to be used here in accordance with the expression of the formula (24) α has no effect on the result due to $D_L = \sigma^\alpha$ and $D_L = 0$.

(B) If $D_G \to 0$ expression (24) turns into the well-known Cauchy distribution

$$p(x,t)|_{\alpha=1} = \frac{1}{\pi} \frac{D_L t}{D_L^2 t^2 + x^2}, \quad D_G \to 0. \tag{26}$$

3.2. Power-law asymptotic around the tails of the PDF

The asymptotic behaviour of the PDF $p(x,t)$ at large x are determined by the first non-analytical term in the series expansion of the exponent in expression (22) [25],

$$p\left(|x| \to \infty, t\right) \sim -\int_{-\infty}^{+\infty} \frac{dk}{2\pi} \exp\left(-ikx\right)\left(D_L|k|^\alpha t + D_G k^2 t\right)$$

$$= -\int_{-\infty}^{+\infty} \frac{dk}{2\pi} \exp\left(-ikx\right)\left(D_L|k|^\alpha t\right) = \frac{D_L t \, \sin\left(\pi\alpha/2\right) \Gamma\left(\alpha + 1\right)}{\pi|x|^{1+\alpha}}. \tag{27}$$

In equation (27) we use the value of the following improper integral

$$\int_0^\infty dt \, t^{\alpha+2m} e^{-it} = (-1)^{m+1} i e^{-i(\alpha\pi/2)} \Gamma(\alpha + 2m + 1), \quad m = 0, 1, 2, \ldots. \tag{28}$$

Equation (27) shows that $p(x,t)$ is a power-law function for larger x, and the power-law exponent is $-(\alpha + 1)$. Taking the logarithm on both sides of relation (27) we get

$$\lim_{|x|\to\infty} \log_{10} p(x,t) = \log_{10} \frac{D_L t \, \sin(\pi\alpha/2)\Gamma(\alpha + 1)}{\pi} - (\alpha + 1)\log_{10}|x|. \tag{29}$$

This result shows that $\log_{10} p(|x| \to \infty, t)$ is a linear function of $\log_{10}|x|$ with the slope $-(\alpha + 1)$, i.e., we can represent the power-law relationship between $p(x,t)$ and large x through log–log plots. Then, in the numerical results parts (figure 1 to figure 3), an auxiliary line with slope equal to the power-law exponent is included to verify the power-law relationship in (29).

The asymptotic decay of the tails of pure Lévy processes is $p(x) \simeq |x|^{-(1+\alpha)}$ [21, 27]. Comparing the power-law asymptotic of the pure Lévy process and the process (27) combining Gaussian and Lévy noises we conclude that the asymptotic of the combined noise case asymptotically only depends on the Lévy noise index. This can be easily understood in view of the independence of these two kinds of noise, as well as the absence of the heavy-tailed asymptotic of the pure Gaussian case. As we will see, the intermediate x-behaviour does carry signatures of the Gaussian noise.

At the end of this subsection we briefly dwell on the mean squared displacement and fractional moments for the considered FFPKE (20) and the influence of both types of noise on these quantities. First, due to the power law decay (29) of the PDF the mean squared displacement does not exist, and one has to characterise the diffusion process with fractional moments $\langle |x|^q \rangle$. For pure BM and pure LFs the fractional moments scale as $t^{q/2}$ for any q and $t^{q/\alpha}$ for $q < \alpha < 2$, respectively [22], displaying the superdiffusive behaviour of LFs. It was shown in [66, 67] that
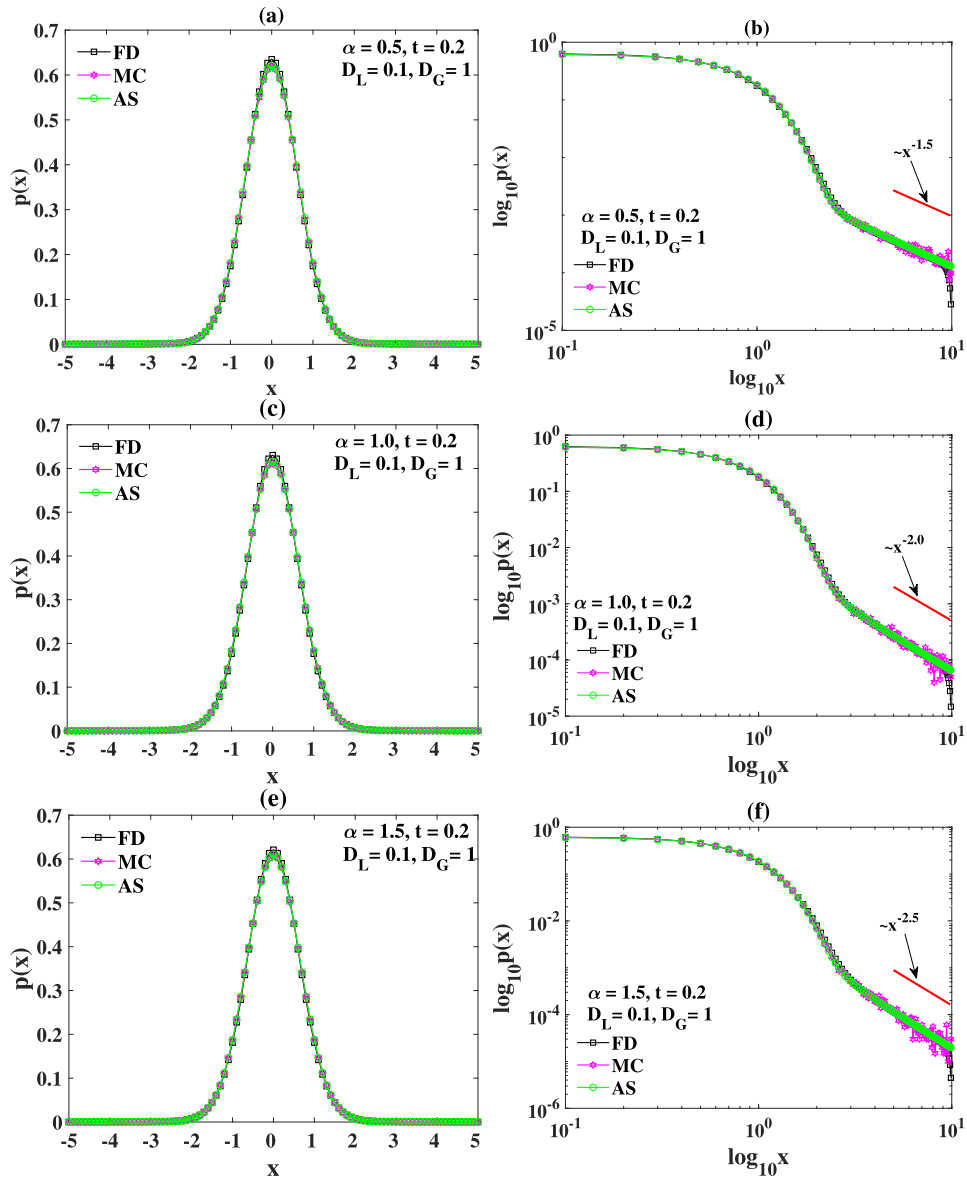
Figure 1. PDF $p(x, t)$ obtained from the FD, Monte Carlo (MC) simulations, and the analytical solution for $D_L = 0.1$, $D_G = 1$, $t = 0.2$, and $U(x) = $ const. (a) $\alpha = 0.5$ and (b) the corresponding log–log plot; (c) $\alpha = 1.0$ and (d) the corresponding log–log plot; (e) $\alpha = 1.5$ and (f) the corresponding log–log plot.

for the combined Lévy–Brownian process governed by the FFPKE (20) fractional moments behave as $t^{q/2}$ at short times (pure Brownian behaviour) and as $t^{q/\alpha}$ at long times, that is, it displays pure Lévy behaviour in the long time limit. Such a crossover from normal to superdiffusive scaling is a particular case of the phenomenon called 'accelerating superdiffusion'. For the details of this and other phenomena in a general context of the distributed order fractional kinetics we refer the reader to [66–70].
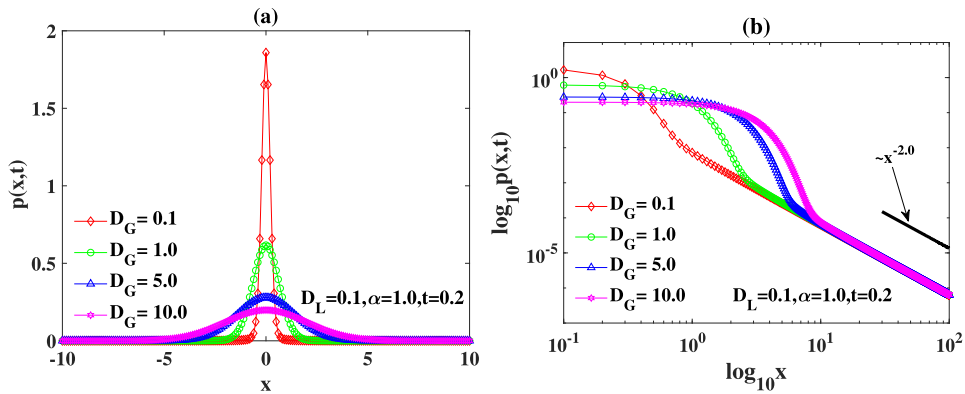
Figure 2. PDF $p(x, t)$ with $D_L = 0.1$ and different values $D_G = 0.1, 1.0, 5.0, 10.0$, at time $t = 0.2$. (a) Linear–linear plot; (b) log–log plot.

3.3. Numerical results

Comparisons between the analytical solution of $p(x, t)$, results from Monte Carlo (MC) simulations of the underlying SDE, and the result obtained from the finite difference method (FD) are presented in figure 1 for the special cases $\alpha = 0.5$, $\alpha = 1.0$, and $\alpha = 1.5$ for $t = 0.2$. In this figure the analytical solutions in the real space are calculated through the inverse Fourier transformation of equation (22). The FD is used to solve the FFPKE (20). In figure 1 panels (a), (c), and (e) show linear scales, while the corresponding panels (b), (d), and (f) display the results in log–log scale. The auxiliary lines indicate that the power-tails of the PDF $p(x, t)$ is fully consistent with result (27).

Figure 2 shows the PDF for $D_L = 0.1$ and different values of D_G. Panel (a) shows the results on linear scales and panel (b) is the corresponding log–log plot. Figure 2(a) indicates that a larger noise intensity D_G leads to lower peaks of the PDF while the PDF is getting broader around the origin. Interestingly, as predicted by the theoretical result (29), the tails for all cases are identical and thus only depend on the noise intensity D_L and stability parameter α. As expected the slope in figure 2(b) is $-(\alpha + 1) = -2.0$.

Figure 3 is a log–log representation of the PDF $p(x, t)$ for different times. In each panel of figure 3, the results $p(x, t)$ are obtained through the difference solution of equation (20). In the FD, the stability index $\alpha = 1.5$, noise intensity $D_G = 1.0$, and different values for D_L, time step $dt = 0.001$, and spatial increment $dx = 0.01$ were used. In each panel the PDF $p(x, t)$ has a Gaussian shape for the case $D_L = 0$, while we see distinct power-law tails for the combined noise cases ($D_L \neq 0$). We note that larger D_L values leads to heavier tails of the PDF for the combined-noise cases with the same D_G. In addition, comparing panels (a) to (d) we find that longer times t lead to the heavier tails at the same x-value in the tail regions.

4. Fractional Fokker–Planck–Kolmogorov equation with harmonic external potential

We now turn to the solution of the FFPKE (19) in the presence of an external harmonic potential. The stationary analytical solutions are available for some special cases and the power-law asymptotic of the stationary solution are proved. We note that the FFPKE (19) is more complicated for the case of a non-constant external potential, and we concentrate on the more easily
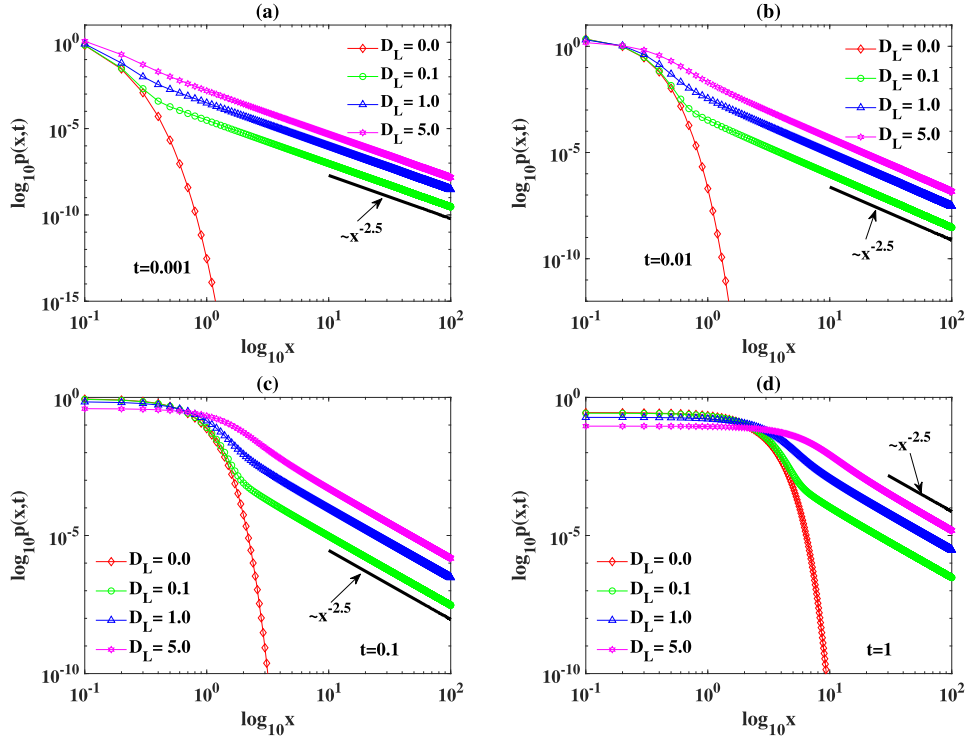
Figure 3. Log–log plots of the PDF $p(x,t)$ at times $t = 0.001, 0.01, 0.1$, and 1.0 for $\alpha = 1.5$ and $D_G = 1.0$.

accessible stationary case $p_{st}(x)$ of the equation instead of the full time-dependent solution $p(x,t)$.

4.1. Analytical solutions

We here derive the stationary solution in the Fourier space and obtain explicit solutions in the real space for the special cases $\alpha = 2$ and $\alpha = 1$. For the harmonic potential function $U(x) = x^2/2$ the PDF $p(x,t)$ satisfies the FFPKE

$$\frac{\partial}{\partial t}p(x,t) = \frac{\partial}{\partial x}[xp(x,t)] + D_L\frac{\partial^\alpha}{\partial|x|^\alpha}p(x,t) + D_G\frac{\partial^2}{\partial x^2}p(x,t). \tag{30}$$

In the Fourier space $Z_X(k,t)$ thus satisfies

$$\frac{\partial}{\partial t}Z_X(k,t) = -k\frac{\mathrm{d}Z_X(k,t)}{\mathrm{d}k} - D_L|k|^\alpha Z_X(k,t) - D_G k^2 Z_X(k,t), \tag{31}$$

where, $Z_X(k,t)$ is the Fourier transformation of $p(x,t)$. Note that $Z_X(k,0) = 1$. By the method of characteristics, the solution of equation (31) is [21]

$$Z_X(k,t) = \exp\left(-\frac{D_L|k|^\alpha}{\alpha}[1 - \mathrm{e}^{-\alpha t}] - \frac{D_G k^2}{2}[1 - \mathrm{e}^{-2t}]\right). \tag{32}$$

We can then always get the stationary solution $Z_X(k)$ as (note that we omit 'st' for $Z_X(k)$)

$$Z_X(k) = \exp\left(-\frac{D_L}{\alpha}|k|^\alpha - \frac{D_G}{2}k^2\right). \tag{33}$$

By inverse Fourier transformation of equation (33) we get the stationary PDF $p_{st}(x)$ in real space. This transformation is difficult, and we are able to perform it for the special cases $\alpha = 2$ and $\alpha = 1$.

For the case $\alpha = 2$, the analytical solution can be obtained by inverse Fourier transformation of $Z_X(k) = \exp(-D_L|k|^2/2 - D_G k^2/2)$,

$$p_{st}(x)|_{\alpha=2} = \frac{1}{\sqrt{2\pi(D_L + D_G)}} \exp\left(-\frac{x^2}{2(D_L + D_G)}\right). \tag{34}$$

For the case $\alpha = 1$, the inverse Fourier transformation of $Z_X(k) = \exp(-D_L|k| - D_G k^2/2)$ produces

$$p_{st}(x)|_{\alpha=1} = \frac{1}{\sqrt{8\pi D_G}} \left[\exp\left(\frac{(D_L + ix)^2}{2D_G}\right) \text{erfc}\left(\frac{D_L + ix}{\sqrt{2D_G}}\right) + \text{c.c}\right], \tag{35}$$

where, again, c.c is the complex conjugate of the first part in the curly brackets on the right hand side of equation (35) and $\text{erfc}(x)$ is the complementary error function. There are two special cases of equation (35) that are worth mentioning:

(A) If only Gaussian noise exists, that is, $D_L = 0$, equation (35) reduces to the Gaussian distribution $p_{st}(x)|_{\alpha=1} = \exp(-x^2/[2D_G])/\sqrt{2\pi D_G}$.

(B) If $D_G \to 0$, then $p_{st}(x)|_{\alpha=1} \to (1/\pi)D_L/(D_L^2 + x^2)$, the well-known Cauchy distribution.

4.2. Power-law asymptotic around the tails of the stationary PDF

The power-law asymptotic of the stationary PDF $p_{st}(x)$ at large x can be proved in the same way as in the constant-potential case, namely,

$$\lim_{|x|\to\infty} p_{st}(x) \sim -\int_{-\infty}^{+\infty} \frac{dk}{2\pi} \exp(-ikx)\left(\frac{D_L}{\alpha}|k|^\alpha + \frac{D_G}{2}k^2\right)$$
$$= -\int_{-\infty}^{+\infty} \frac{dk}{2\pi} \exp(-ikx)\frac{D_L}{\alpha}|k|^\alpha = \frac{D_L \sin(\pi\alpha/2)\Gamma(\alpha)}{\pi|x|^{1+\alpha}}. \tag{36}$$

This shows that $p_{st}(|x| \to \infty)$ is a power-law function of $|x|$, that is, $\log_{10} p_{st}(|x| \to \infty)$ and $\log_{10}|x|$ have a linear relationship. Moreover, equation (36) exhibits that larger D_L values leads to larger amplitudes of $p_{st}(|x| \to \infty)$, which means a heavier tail of the stationary PDF.

For the SDE with pure α-stable Lévy noise and confining the potential $U(x) = x^2/2$ the stationary PDFs have power-law asymptotic of the form $|x|^{-(\alpha+1)}$ at $|x| \to \infty$ [55]. Comparing with the power-law asymptotic of the combined noise case, equation (36), we find the same power-law asymptotic. Solely from the tails the presence of the Gaussian noise therefore cannot be discerned, as detailed in the numerical analysis below.

4.3. Numerical results

The analytical solution of the stationary PDF obtained from the inverse Fourier transformation of relation (33) is compared with the results of the FD in figure 4. In the numerical calculation of the FD the time and space steps are $dt = 0.01$ and $dx = 0.1$, respectively. Good agreement
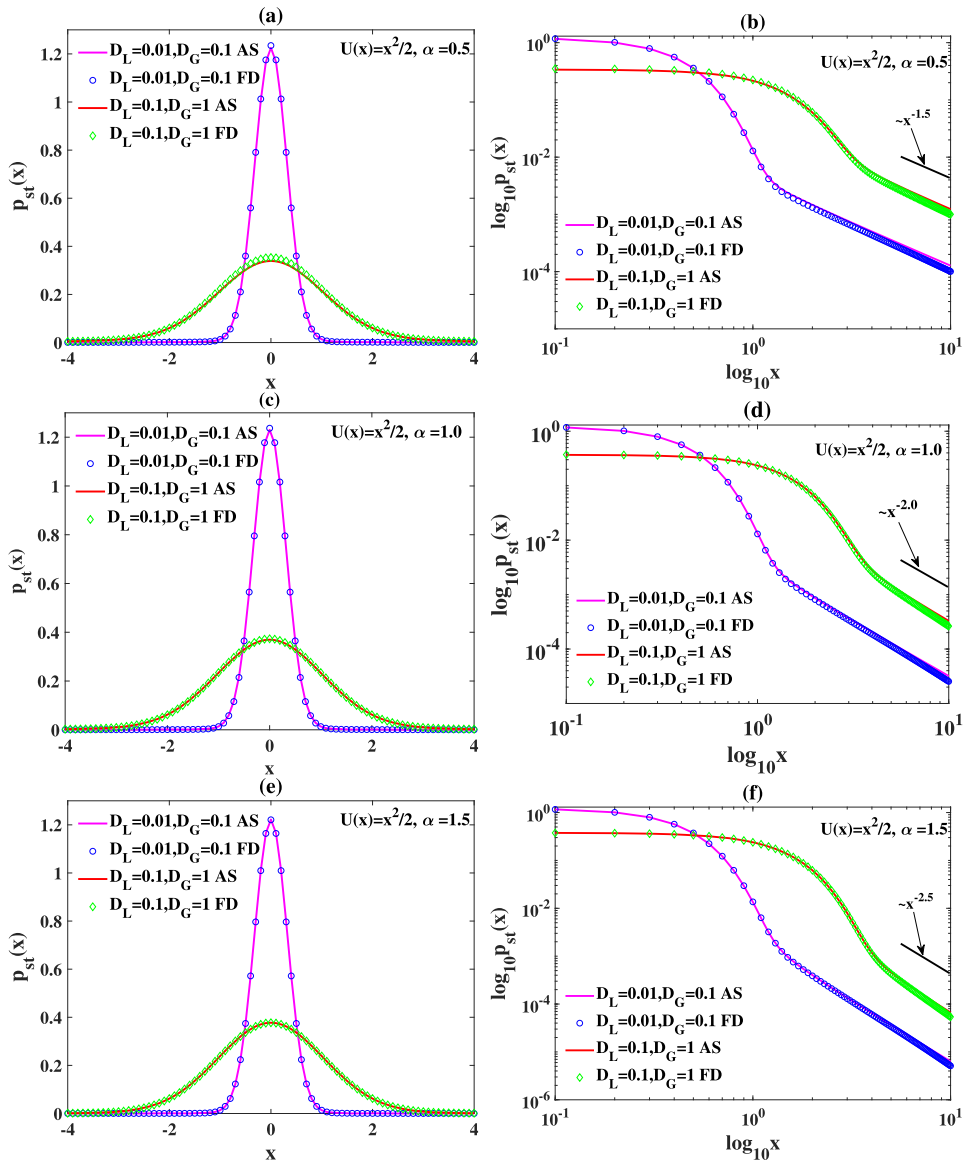
Figure 4. Stationary PDFs obtained from the finite difference (FD) method, compared with the analytical solution for the harmonic external potential $U(x) = x^2/2$. Panels (a) and (b) are for $\alpha = 0.5$ in linear and log–log scales; (c) and (d) are correspondingly for $\alpha = 1.0$; and (e) and (f) are for $\alpha = 1.5$.

between the stationary PDF and the finite difference results are observed in figure 4. In the log–log plots the power-law asymptotic are distinct, and consistent with the theoretical results (36). Moreover, we see that the noise intensity affects the value of the stationary PDF but does not affect the power-law behaviour.

Figure 5(a) shows the stationary PDF comparison of the pure Gaussian case ($D_L = 0$), for pure Lévy noise ($D_G = 0$), and for the combined-noise case for $U(x) = x^2/2$ and $\alpha = 1.5$ on
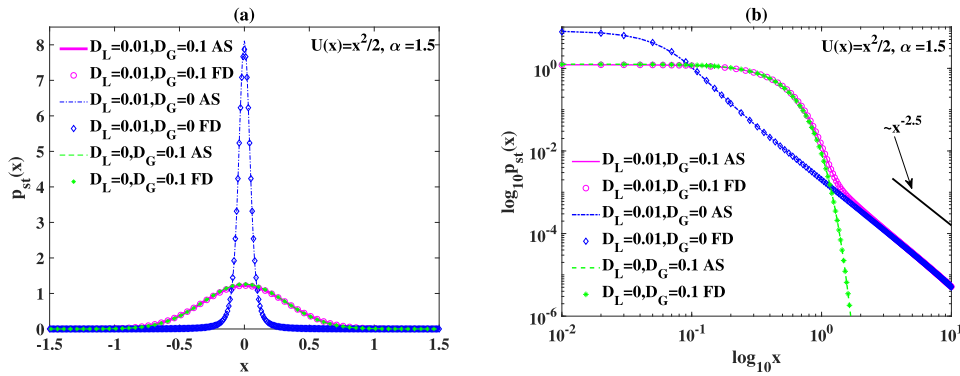
Figure 5. Stationary PDF comparing among pure Gaussian, pure Lévy, and the combined-noise case for $U(x) = x^2/2$ and $\alpha = 1.5$.

both linear and log–log scales. The numerical solutions are obtained through the FD on the interval $[-30, 30]$, with the time step $dt = 0.01$ and space increment $dx = 0.01$. The analytical solutions are obtained from the equation (33) through the inverse Fourier transformation. Figure 5(a) indicates that the numerical solutions fit well the analytical solutions. Figure 5(b) highlights the tails of the PDF. For the pure Gaussian-noise case ($D_L = 0$) we see a fast Gaussian decay, see formula (36). However, both cases of combined-noise and pure Lévy noise case have the same asymptotic tails.

5. Fractional Fokker–Planck–Kolmogorov equation in the presence of quartic and strongly nonlinear potentials

We now study the solution of the FFPKE (19) for the quartic external potential $U(x) = x^4/4$ and the 'strongly nonlinear' potential $U(x) = x^{2m+2}/(2m+2)$ with $m = 2, 3, 4, \dots$. We again limit our discussion to the stationary solution. Specifically, we find the stationary analytical solutions of the special cases $D_L = 0$ and $D_G = 0$ with $\alpha = 1$ and $U(x) = x^4/4$. Moreover, the power-law asymptotic about the tails of the stationary PDF is proved and presented through log–log plots in our numerical analysis.

5.1. Analytical solutions

For the case $U(x) = x^{2m+2}/(2m+2)$ $(m = 1, 2, \dots)$, the stationary distribution $p_{st}(x)$ satisfies

$$\frac{\partial}{\partial x}\left(x^{2m+1}p_{st}(x)\right) + D_L\frac{\partial^\alpha}{\partial|x|^\alpha}p_{st}(x) + D_G\frac{\partial^2}{\partial x^2}p_{st}(x) = 0. \tag{37}$$

In the Fourier space equation (37) can be expressed as (note that we again omit the subscript 'st' for $Z_X(k)$)

$$\frac{d^{2m+1}Z_X(k)}{dk^{2m+1}} = D_L\,\text{sign}(k)|k|^{\alpha-1}Z_X(k) + D_G k Z_X(k). \tag{38}$$

In general, the analytical solutions for both equations (37) and (38) are difficult to derive. We obtain the analytical solutions for the following two special cases:

14
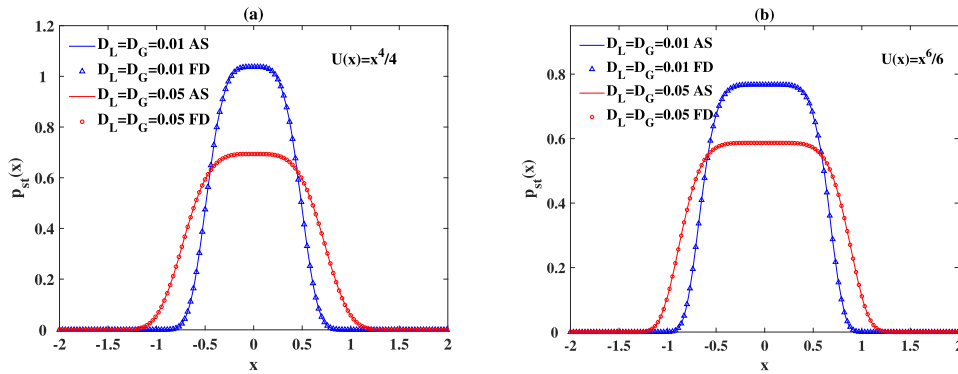
Figure 6. Stationary PDFs obtained from finite difference method compared with the AS for $\alpha = 2$. (a) $U(x) = x^4/4$, (b) $U(x) = x^6/6$.

(A) For the stability index $\alpha = 2$ the AS of (37) is

$$p_{st}(x) = \frac{m+1}{\Gamma(1/[2m+2])[(2m+2)(D_L + D_G)]^{1/(2m+2)}} \times \exp\left(-\frac{1}{D_L + D_G} \frac{x^{2m+2}}{2m+2}\right). \quad (39)$$

(B) For the special case $\alpha = 1$, $U(x) = x^4/4$ and $D_G = 0$ the stationary distribution in the Fourier space satisfies

$$\frac{d^3 Z_X(k)}{dk^3} = D_L \, \text{sign}(k) Z_X(k), \quad (40)$$

and the solution for the pure Lévy case can be obtained as

$$Z_X(k) = \frac{2}{\sqrt{3}} \exp\left(-\frac{D_L^{1/3}}{2}|k|\right) \cos\left(\frac{D_L^{1/3}\sqrt{3}}{2}|k| - \frac{\pi}{6}\right). \quad (41)$$

After inverse Fourier transformation of equation (41) we have

$$p_{st}(x) = \frac{1}{\pi} \frac{D_L}{x^4 + D_L^{4/3} - D_L^{2/3} x^2}. \quad (42)$$

And the exact stationary PDFs for $\alpha = 1, D_G = 0$ and arbitrary m can be found in [30]

Figure 6 presents the stationary solution $p_{st}(x)$ for the quartic and x^6 potentials for different noise intensities for the case $\alpha = 2$. The analytical solutions are compared with the finite difference solutions for the cases $D_L = D_G = 0.01$ and $D_L = D_G = 0.05$, in each panel. Both results agree well in all cases. For the FD, the parameters $dx = 0.01$ and $dt = 0.01$ were used on the interval $x \in [-5, 5]$. We find that smaller D_L and D_G lead to a thinner PDF. Moreover, $U(x) = x^4/4$ results in a thinner PDF than for $U(x) = x^6/6$ for the same noise intensity.

In figure 7 the stationary analytical solution (42) is compared with the corresponding finite difference solution for $D_G = 0$, $D_L = 0.05$ and $\alpha = 1.0$. In the finite difference scheme the parameter $dx = 0.005$, $dt = 0.01$ and the interval $x \in [-20, 20]$ are employed. Figure 7(a) shows that the analytical solution agrees well with the finite difference solution. Panel (b) displays the corresponding log–log plot with the power-law tails of the PDF, detailing the asymptotic for the pure Lévy case with $D_G = 0$, $\lim_{|x|\to\infty} p(x) \simeq x^{-4}$, compare the analytical solution (42). In panel (b) of figure 7 the auxiliary line with slope -4 is plotted with the
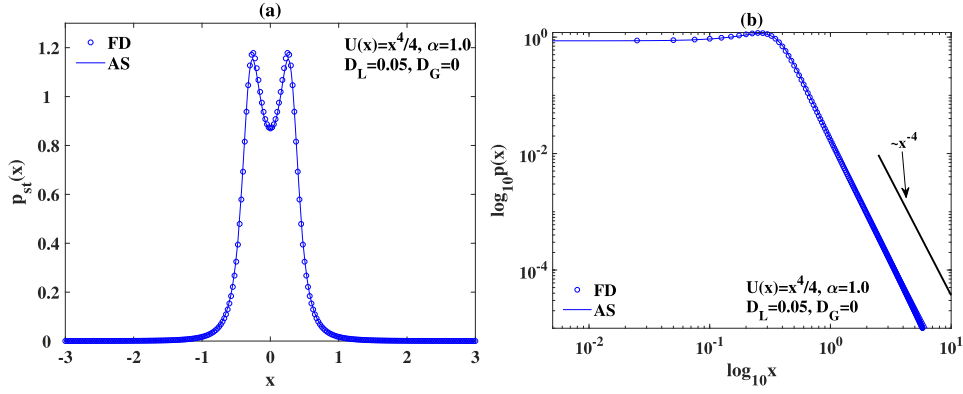
Figure 7. Stationary PDFs comparing between the finite difference solution (FD) and the analytical solution for $D_G = 0$, $D_L = 0.05$, and $\alpha = 1.0$.

expected power-law asymptotic. Notably, panel (a) of figure 7 demonstrates a bimodal stationary PDF, with a distinct dip towards the origin, $x = 0$. This behaviour for Lévy stable processes was first analysed in a series of works [25–29]. We will here analyse how this phenomenon is when we use combined Lévy–Gaussian noise.

5.2. Power-law asymptotic around the tails of the stationary PDF

The power-law asymptotic of the stationary solution is analysed theoretically through the method laid out in [27]. For the potential $U(x) = x^{2m+2}/(2m+2)$ $(m = 0, 1, 2, \ldots)$ the stationary solution satisfies

$$\frac{\partial}{\partial x}(U'(x)p_{st}) + D_L \frac{\partial^\alpha}{\partial |x|^\alpha} p_{st} + D_G \frac{\partial^2}{\partial x^2} p_{st} = 0. \tag{43}$$

We find $p_{st}(x + \Delta x) \simeq p_{st}(x) \simeq p_{st}(x - \Delta x)$ and $D_-^\alpha p_{st}(x) \ll D_+^\alpha p_{st}(x)$, when $x \to +\infty$. To prove the power-law asymptotic we distinguish the two different cases $\alpha \neq 1$ and $\alpha = 1$:

(A) When $\alpha \neq 1$ then the stationary solution meets

$$\frac{\partial}{\partial x}(U'(x)p_{st}(x)) - \frac{D_L}{2 \cos(\pi\alpha/2)\Gamma(2-\alpha)} \frac{d^2}{dx^2} \int_{-\infty}^x \frac{p_{st}(\xi)}{(x-\xi)^{\alpha-1}} d\xi \simeq 0, \quad x \to \infty \tag{44}$$

for $1 < \alpha < 2$, namely,

$$x^{2m+1} p_{st}(x) \simeq \frac{D_L}{2 \cos(\pi\alpha/2)\Gamma(2-\alpha)} \frac{d}{dx} \int_{-\infty}^x \frac{p_{st}(\xi)}{(x-\xi)^{\alpha-1}} d\xi, \quad x \to +\infty, 1 < \alpha < 2. \tag{45}$$

Suppose that the asymptotic behaviour of $p_{st}(x)$ satisfies $p_{st}(x) \sim C_1/x^\mu$ $(x \to +\infty, \mu > 0)$, and then integrate equation (45) to get

$$\frac{2C_1 \cos(\pi\alpha/2)\Gamma(2-\alpha)}{D_L(2m+2-\mu)} x^{2m+2-\mu} \simeq \int_{-\infty}^x \frac{p_{st}(\xi)}{(x-\xi)^{\alpha-1}} d\xi. \tag{46}$$

Then the approximated value for the right-hand side integral can be obtained as

$$\int_{-\infty}^{x} \frac{p_{st}(\xi)}{(x-\xi)^{\alpha-1}}d\xi \simeq \frac{1}{x^{\alpha-1}} \int_{-\infty}^{x} p_{st}(\xi)d\xi \simeq \frac{1}{x^{\alpha-1}} \int_{-\infty}^{\infty} p_{st}(\xi)d\xi = \frac{1}{x^{\alpha-1}}. \quad (47)$$

Comparing equations (46) and (47) we see that

$$\mu = \alpha + 2m + 1, \quad (48)$$

and

$$C_1 = \frac{D_L(2m+2-\mu)}{2 \cos(\pi\alpha/2)\Gamma(2-\alpha)} = \frac{D_L \sin(\pi\alpha/2)\Gamma(\alpha)}{\pi}. \quad (49)$$

In view of the symmetry of the stationary solution its power-law asymptotic form is

$$p_{st}(x) \sim \frac{D_L \sin(\pi\alpha/2)\Gamma(\alpha)}{\pi|x|^{\alpha+2m+1}}, \quad |x| \to \infty, \ 1 < \alpha < 2. \quad (50)$$

For the case $0 < \alpha < 1$, μ has the identical value (48), and

$$C_1 = \frac{D_L}{2 \cos(\pi\alpha/2)\Gamma(1-\alpha)} = \frac{D_L \sin(\pi\alpha/2)\Gamma(\alpha)}{\pi}. \quad (51)$$

Thus, the general power-law asymptotic of $\alpha \neq 1$ becomes

$$p(x) \sim \frac{D_L \sin(\pi\alpha/2)\Gamma(\alpha)}{\pi|x|^{\alpha+2m+1}}, \quad |x| \to \infty, \ 0 < \alpha < 2, \alpha \neq 1. \quad (52)$$

(B) When $\alpha = 1$ the stationary solution satisfies

$$\frac{\partial}{\partial x}(U'(x)p_{st}(x)) - D_L\frac{1}{\pi}\frac{d}{dx}\int_{-\infty}^{\infty} \frac{p_{st}(\xi)}{x-\xi}d\xi \simeq 0. \quad (53)$$

After the same procedure followed in part (A) the asymptotic of the stationary solution turns into

$$p_{st}(x) \sim \frac{D_L}{\pi|x|^{2m+2}}, \quad |x| \to \infty, \quad (54)$$

which is indeed a special case of result (50) when $\alpha = 1$.

Thus, the power-law asymptotic of stationary solution uniquely satisfies

$$p_{st}(x) \sim \frac{D_L \sin(\pi\alpha/2)\Gamma(\alpha)}{\pi|x|^{\alpha+2m+1}}, \quad |x| \to \infty, \ 0 < \alpha < 2. \quad (55)$$

Equation (55) shows that the Gaussian noise intensity D_G has no effect on the power-law asymptotic of the PDF, and thus for the pure Lévy case, the PDF has the same power-law asymptotic as reported in [25].
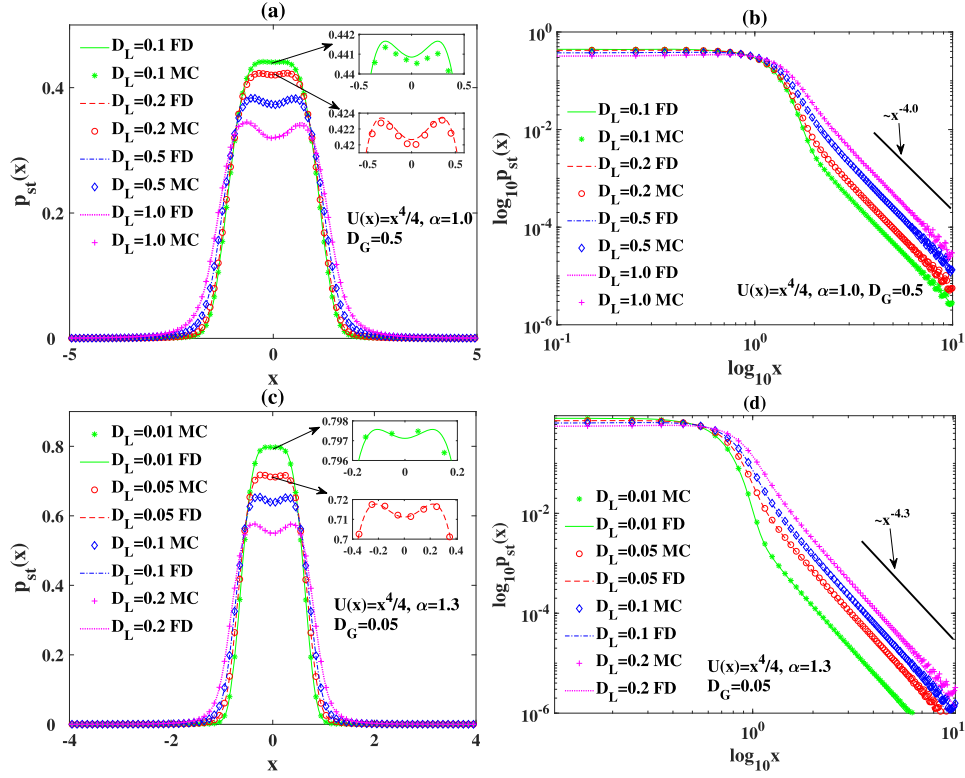
Figure 8. Stationary PDF from the FD and Monte Carlo (MC) solution for $U(x) = x^4/4$. (a) is for $\alpha = 1.0$ and (b) is the corresponding plot on log–log scale. (c) is for $\alpha = 1.3$, with the corresponding log–log representation in (d).

5.3. Numerical results

In this subsection we present our numerical results for the external potentials $U(x) = x^4/4$ and $U(x) = x^6/6$. Both Monte Carlo solutions for the SDE and finite difference solutions for the FFPKE are used.

Figure 8 presents the stationary PDFs for different noise strengths D_L and D_G for the quartic potential $U(x) = x^4/4$, in both linear and log–log representation. In the latter the power-law tails are highlighted. For the FD the time step $dt = 0.01$ and spatial increment $dx = 0.01$ are adopted. The finite difference solution agrees well with the Monte Carlo solution. Figures 8(a) and (c) show that larger D_L lead to a stronger bimodality of the PDF for the same D_G. The bimodality of the stationary PDF for smaller D_L is shown in the zoom-in in the insets in figuress 8(a) and (c). Panels (b) and (d) are the corresponding double-logarithmic plots detailing the power-law asymptotic for the tails of the PDF. For the case $U(x) = x^4/4$ and $\alpha = 1$, figure 8(b) shows that the tails of the PDF satisfy $p_{st}(x) \simeq x^{-4}$ ($x \to +\infty$). Similarly, for $\alpha = 1.3$ panel (d) shows that the tails of the PDF satisfy $p_{st}(x) \simeq x^{-4.3}$ for ($x \to +\infty$). Both results are thus consistent with equation (55) where the tails of the stationary PDF are shown to obey $p_{st}(x) \simeq |x|^{-(\alpha+3)}$ at $x \to \infty$. Moreover, we find that larger D_L lead to heavier tails in each of the log–log plots.

Figure 9 shows the stationary PDF on both linear and double-logarithmic scales for different noise strengths D_L and D_G for the case of the strongly nonlinear potential $U(x) = x^6/6$.
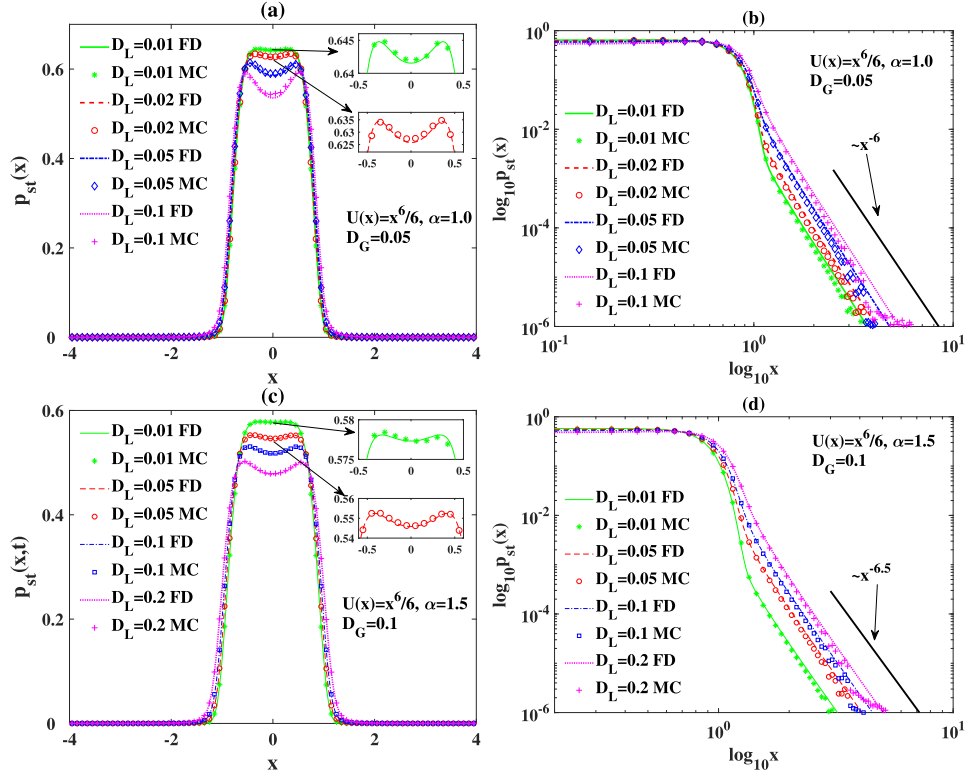
Figure 9. Stationary PDF from the FD and Monte Carlo (MC) solution for $U(x) = x^6/6$. (a) is for $\alpha = 1.0$ with the corresponding log–log representation in (b). (c) is for $\alpha = 1.3$, with log–log scales in (d).

Both finite difference solutions and Monte Carlo solutions are shown, demonstrating good agreement. For the FD the time step was $dt = 0.01$ and the spatial increment was $dx = 0.01$. Figures 9(a) and (c) show that larger D_L values lead to a stronger bimodality of the PDF for the same D_G. The bimodality for smaller D_L is shown in the insets. Panels (b) and (d) show that the tails of the PDF have power-law asymptotic. For the case $U(x) = x^6/6$ equation (55) indicates that $p_{st}(x) \simeq |x|^{-(\alpha+5)}$ as $|x| \to \infty$. Namely, $\log_{10} p_{st}(x) \simeq -(\alpha + 5)\log_{10}|x|$ as $|x| \to \infty$, such that in the log–log plot the stationary PDF has the asymptotic slope $-(\alpha + 5)$. For $\alpha = 1$, $p_{st}(x) \simeq |x|^{-6}(|x| \to \infty)$, and the tails of the PDF are indeed parallel to the auxiliary line with slope -6 in panel (b). In panel (d) the auxiliary line has slope -6.5, again consistent with the analytical prediction.

6. Fractional Fokker–Planck–Kolmogorov equation in the presence of an external subharmonic potential

In this section, consider the FFPKE (19) in the presence of a 'subharmonic' potential $U(x) = |x|^c/c$ ($0 < c < 2$). Specifically, the FFPKE can be expressed as

$$\frac{\partial}{\partial t}p(x,t) = \frac{\partial}{\partial x}\left(|x|^{c-1}\,\text{sign}(x)p(x,t)\right) + D_L\frac{\partial^\alpha}{\partial|x|^\alpha}p(x,t) + D_G\frac{\partial^2}{\partial x^2}p(x,t), \quad (56)$$
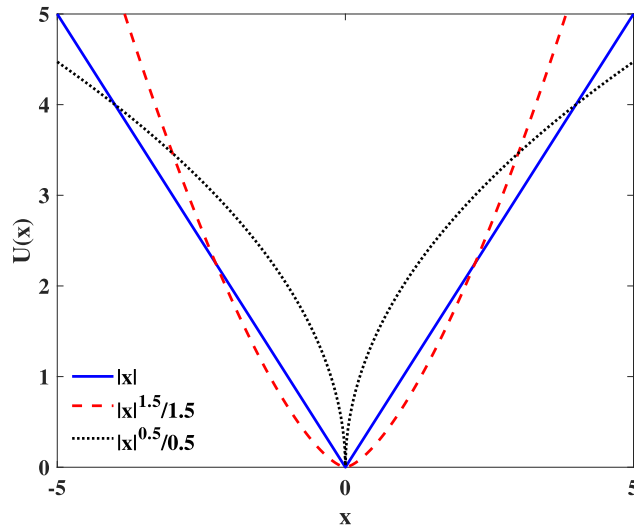
Figure 10. Examples for subharmonic potentials $U(x) = |x|^c/c$ with $0 < c < 2$ for the parameters $c = 1.0$, $c = 1.5$, and $c = 0.5$.

where sign(x) is the sign function. In figure 10 the subharmonic potential functions with some specific parameters are presented. We discuss the existence of a stationary state and determine the power-law asymptotic of the tails of the stationary PDF.

6.1. Existence of a stationary PDF and corresponding power-law tails

We here prove that the tails of the stationary PDF have power-law asymptotic. To this end we use the same method as employed in section 5.2.

If a stationary state of equation (56) exists, it satisfies

$$\frac{\partial}{\partial x}\left(|x|^{c-1}\,\text{sign}(x)p_{\text{st}}(x)\right) + D_{\text{L}}\frac{\partial^\alpha}{\partial|x|^\alpha}p_{\text{st}}(x) + D_{\text{G}}\frac{\partial^2}{\partial x^2}p_{\text{st}}(x) = 0. \tag{57}$$

Considering that the stationary solution satisfies $p_{\text{st}}(x + \Delta x) \simeq p_{\text{st}}(x) \simeq p_{\text{st}}(x - \Delta x)$ for $|x| \to \infty$, according to the definition of the Riemann–Liouville derivatives (8) we find that $D_-^\alpha p_{\text{st}}(x) \ll D_+^\alpha p_{\text{st}}(x)$ when $x \to +\infty$, and $D_+^\alpha p_{\text{st}}(x) \ll D_-^\alpha p_{\text{st}}(x)$ when $x \to -\infty$. Then, equation (57) reduces to

$$x^{c-1}p_{\text{st}}(x) \simeq \frac{D_{\text{L}}}{2\,\cos(\pi\alpha/2)\Gamma(2-\alpha)}\frac{\text{d}}{\text{d}x}\int_{-\infty}^x\frac{p_{\text{st}}(\xi)}{(x-\xi)^{\alpha-1}}\text{d}\xi, \quad x \to +\infty, \, 1 < \alpha < 2 \tag{58}$$

and, respectively,

$$-(-x)^{c-1}p_{\text{st}}(x) \simeq \frac{D_{\text{L}}}{2\,\cos(\pi\alpha/2)\Gamma(2-\alpha)}\frac{\text{d}}{\text{d}x}\int_x^\infty\frac{p_{\text{st}}(\xi)}{(\xi-x)^{\alpha-1}}\text{d}\xi, \quad x \to -\infty, \, 1 < \alpha < 2. \tag{59}$$

Assuming that the tails of the distribution are given by a power-law, i.e. $p_{st}(x) \sim C_1/|x|^{\mu}$ ($\mu > 0$, $x \to \infty$) we get

$$\frac{2C_1 \ \cos(\pi\alpha/2)\Gamma(2-\alpha)}{D_L(c-\mu)}x^{c-\mu} \simeq \int_{-\infty}^{x} \frac{p_{st}(\xi)}{(x-\xi)^{\alpha-1}}d\xi, \quad x \to +\infty, \ 1 < \alpha < 2 \tag{60}$$

and

$$\frac{2C_1 \ \cos(\pi\alpha/2)\Gamma(2-\alpha)}{D_L(c-\mu)}(-x)^{c-\mu} \simeq \int_{x}^{\infty} \frac{p_{st}(\xi)}{(\xi-x)^{\alpha-1}}d\xi, \quad x \to -\infty, \ 1 < \alpha < 2. \tag{61}$$

The right-hand sides of equations (60) and (61) can be approximated as

$$\int_{-\infty}^{x} \frac{p_{st}(\xi)}{(x-\xi)^{\alpha-1}}d\xi \simeq \frac{1}{x^{\alpha-1}}\int_{-\infty}^{\infty} p_{st}(\xi)d\xi = \frac{1}{x^{\alpha-1}}, \quad x \to +\infty, \ 1 < \alpha < 2 \tag{62}$$

and

$$\int_{x}^{\infty} \frac{p_{st}(\xi)}{(\xi-x)^{\alpha-1}}d\xi \simeq \frac{1}{(-x)^{\alpha-1}}\int_{-\infty}^{\infty} p_{st}(\xi)d\xi = \frac{1}{(-x)^{\alpha-1}}, \quad x \to -\infty, \ 1 < \alpha < 2. \tag{63}$$

Comparing equations (60) and (62), as well as (61) and (63), we obtain

$$c - \mu = 1 - \alpha \tag{64}$$

and,

$$C_1 = \frac{D_L(c-\mu)}{2 \ \cos(\pi\alpha/2)\Gamma(2-\alpha)} = \frac{D_L \ \sin(\pi\alpha/2)\Gamma(\alpha)}{\pi}. \tag{65}$$

Thus, the power-law asymptotic about the tail of the PDF is

$$p_{st}(x) \sim \frac{C_1}{|x|^{\mu}} = \frac{D_L \ \sin(\pi\alpha/2)\Gamma(\alpha)}{\pi|x|^{c+\alpha-1}}, \quad |x| \to \infty, \ 1 < \alpha < 2. \tag{66}$$

In the derivation of the power-law asymptotic (66) the Riemann–Liouville fractional derivatives (8) with stability parameter $1 < \alpha < 2$ are used. For the fractional derivatives with stability parameter $0 < \alpha < 1$ the analogous power-law asymptotic can be obtained as

$$p_{st}(x) \sim \frac{D_L}{2 \ \cos(\pi\alpha/2)\Gamma(1-\alpha)|x|^{c+\alpha-1}} = \frac{D_L \ \sin(\pi\alpha/2)\Gamma(\alpha)}{\pi|x|^{c+\alpha-1}}, \quad |x| \to \infty, \ 0 < \alpha < 1. \tag{67}$$

Finally, the power-law asymptotic in the Cauchy case $\alpha = 1$ is

$$p_{st}(x) \sim \frac{D_L}{\pi|x|^c}, \quad |x| \to \infty, \ \alpha = 1, \tag{68}$$

which can be viewed as a limiting case of the general power-law asymptotic. Taken altogether, the power-law asymptotic in the subharmonic potential becomes

$$p_{st}(x) \sim \frac{D_L \ \sin(\pi\alpha/2)\Gamma(\alpha)}{\pi|x|^{c+\alpha-1}}, \quad |x| \to \infty, \ 0 < \alpha < 2. \tag{69}$$

Moreover, for the pure Lévy case ($D_G = 0$) the tails of the PDF satisfy the same power-law asymptotic [55].
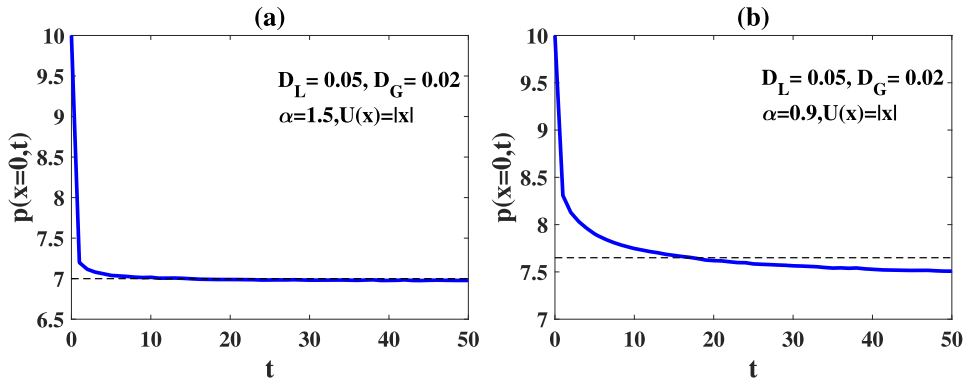
Figure 11. Evolution of the PDF at $x = 0$ as function of time t for $U(x) = |x|$, $D_L = 0.05$, and $D_G = 0.02$. (a) $\alpha = 1.5$, (b) $\alpha = 0.9$.

The PDF $p_{st}(x)$ has to be integrable which implies to $\mu > 1$. The necessary condition for the existence of the steady state therefore is

$$c > 2 - \alpha. \tag{70}$$

Specifically, this means that for the harmonic case $c = 2$ we always have a stationary solution, as proved originally in [21].

6.2. Numerical results

In this section numerical results are presented to verify the condition for the existence of the stationary state and to show the power-law asymptotic of the stationary PDF. Without loss of generality, we choose two special cases, $U(x) = |x|$ ($c = 1$) and $U(x) = |x|^{0.5}/0.5$ ($c = 0.5$). In our presentation the value $p(x = 0, t)$ is selected as a parameter to show the existence of the stationary states, and logarithmic scales are used to show the power-law asymptotic of the stationary solution.

6.2.1. Subharmonic potential $U(x) = |x|$.　We first turn to the case $U(x) = |x|$ for different noise intensities and stability parameter α and verify the necessary condition for the existence of the stationary state with its long-tailed asymptotic $p_{st}(x) \propto |x|^{c+\alpha-1}$ for $|x| \to \infty$.

If the stationary state exists, the PDF will remain unchanged once it arrives at the stationary state. Figure 11 shows the evolution of the PDF at $x = 0$ as function of time. The value of the PDF is obtained through Monte Carlo simulations with the time step $dt = 10^{-3}$ and spatial increment $dx = 0.1$. The number of sample trajectories is 1×10^6 and the initial condition is $x(0) = 0$. In figure 11(a), the PDF $p(x = 0, t)$ first decreases and then remains unchanged when we use the parameters $D_L = 0.05$, $D_G = 0.02$, and $\alpha = 1.5$. This combination of $\alpha = 1.5$ and $c = 1$ meet the necessary condition (70). In contrast, there does not exist a stationary state if (70) is violated. This is demonstrated in figure 11(b). The parameters $\alpha = 0.9$ and $c = 1$ do not satisfy condition (70), and the value of the PDF apparently does not reach a stationary value.

For the case that the stationary state exists, figure 12 shows the value of $p(x = 0, t)$ for different noise intensities. Each panel of figure 12 demonstrates that smaller D_G values lead to higher amplitudes for the same noise intensity D_L. Comparing panels (a) and (b), larger D_L lead to higher amplitudes for the same noise intensities $D_G = 0.01$ and $D_G = 0.05$.
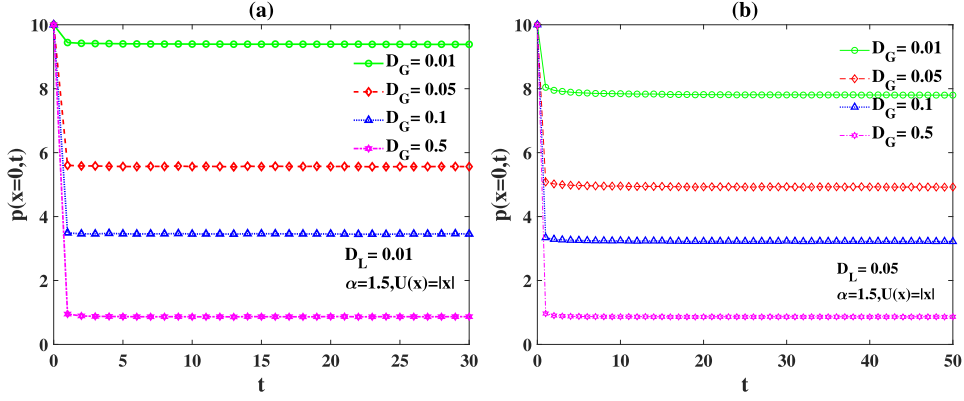
Figure 12. Time evolution of the PDF at $x = 0$ for $U(x) = |x|$ and $\alpha = 1.5$ under different D_{G}. (a) $D_{\mathrm{L}} = 0.01$, (b) $D_{\mathrm{L}} = 0.05$.
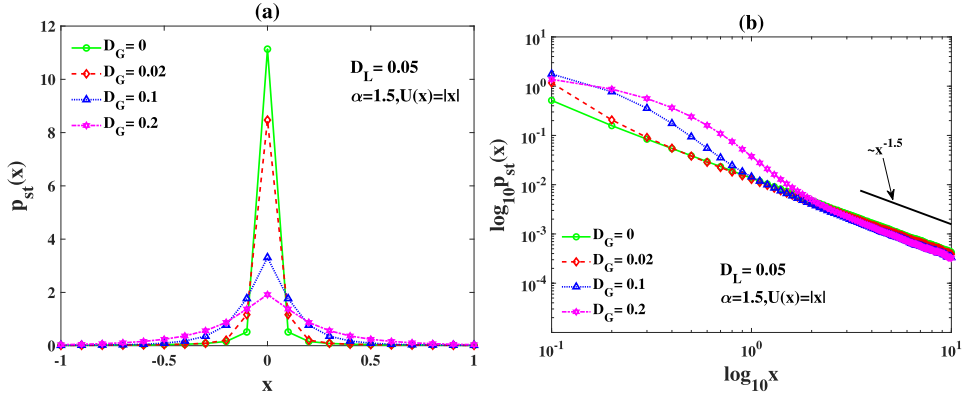
Figure 13. Stationary PDFs and corresponding log–log plots for $U(x) = |x|$, $\alpha = 1.5$, and $D_{\mathrm{L}} = 0.05$.

In section 6.1 the power-law asymptotic of the stationary solution is proved. Figure 13 presents the stationary PDF on linear and log–log scales for $U(x) = |x|$, $\alpha = 1.5$, and $D_{\mathrm{L}} = 0.05$. Panel (a) shows that smaller D_{G} values lead to higher amplitudes. Panel (b) shows that the tails of the stationary PDF satisfy $p_{\mathrm{st}}(x) \simeq |x|^{-1.5}$ as $x \to \infty$. Specifically, we see that the noise intensity D_{G} has no effect on the power-law asymptotic, in accordance with result (66).

6.2.2. Subharmonic potential $U(x) = |x|^{0.5}/0.5$. We now turn to the case $U(x) = |x|^{0.5}/0.5$ and perform a similar analysis.

Figure 14 shows the value $p(x = 0, t)$ of the PDF, obtained from Monte Carlo simulations with the same setting as above, but with initial $x(0) = 1.0$. In figure 14(a) $p(x = 0, t)$ first increases and then decreases to a constant for $\alpha = 1.7$, consistent with the fact that the parameters $\alpha = 1.7$ and $c = 0.5$ satisfy the necessary condition (70) for stationarity. In contrast, for $\alpha = 1.0$, (70) is not satisfied, and panel (b) indeed shows that the stationary state is not reached.

For the case $U(x) = |x|^{0.5}/0.5$ and $D_{\mathrm{L}} = 0.2$ figure 15 shows the effect of the noise intensity on the PDF, where panels (a) and (b) are for $\alpha = 1.7$ and (c) and (d) are for $\alpha = 1.0$. For $\alpha = 1.7$, for which the stationary state exists panel (b) indicates that smaller D_{G} lead to larger
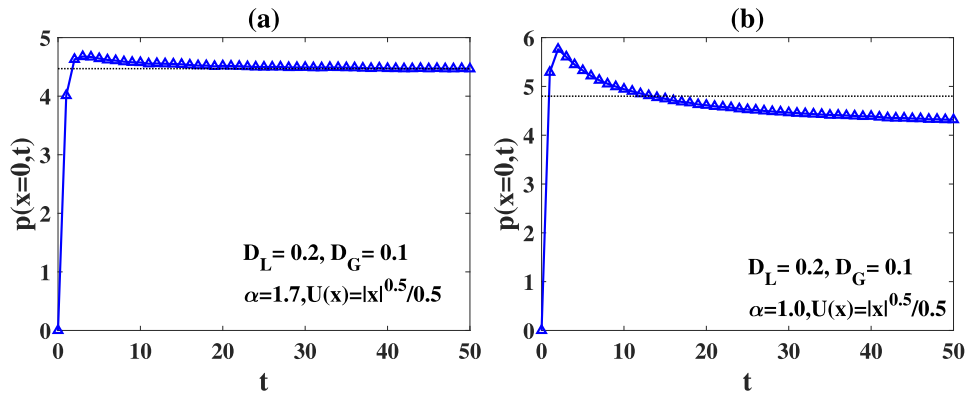
Figure 14. Time evolution of the PDF at $x = 0$ for $U(x) = |x|^{0.5}/0.5$, $D_{\mathrm{L}} = 0.2$, and $D_{\mathrm{G}} = 0.1$. (a) $\alpha = 1.7$, (b) $\alpha = 1.0$.
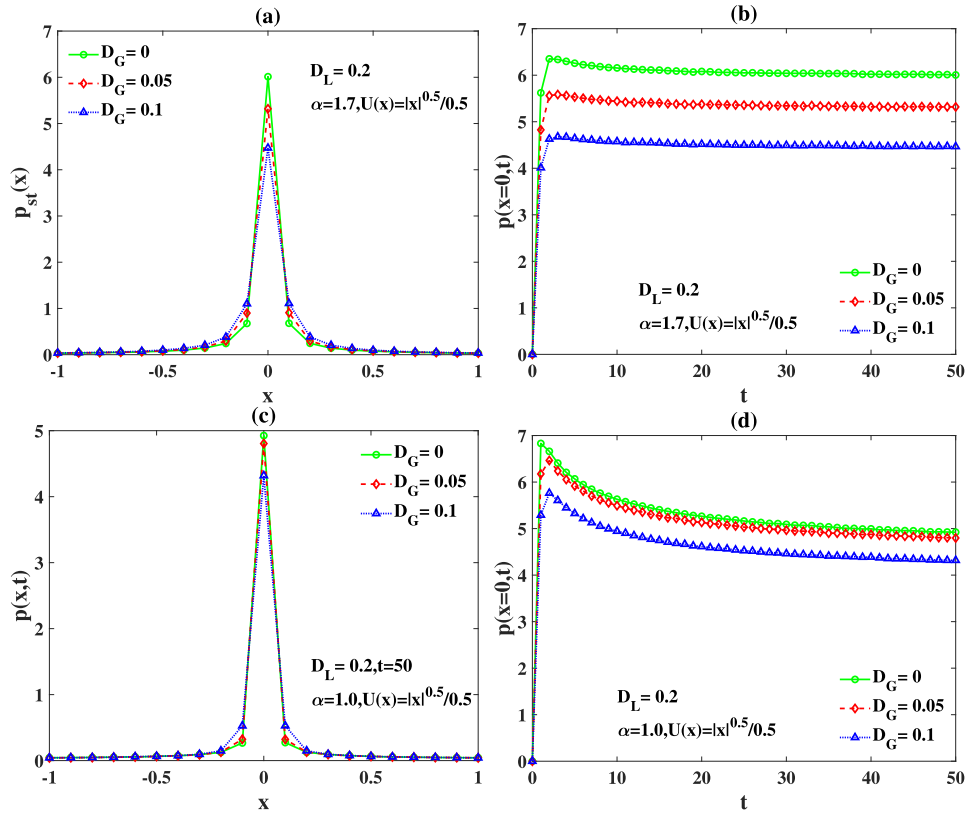
Figure 15. The PDF and time evolution of the PDF at $x = 0$ under different D_{G} for $U(x) = |x|^{0.5}/0.5$ and $D_{\mathrm{L}} = 0.2$. (a) and (b) $\alpha = 1.7$. (c) and (d) $\alpha = 1.0$.

amplitudes of $p(x = 0, t)$ for the same D_{L}, and for all times except $t = 0$. In accordance with the findings of panel (b), panel (a) indicates that smaller D_{G} lead to higher amplitudes $p_{\mathrm{st}}(x = 0)$
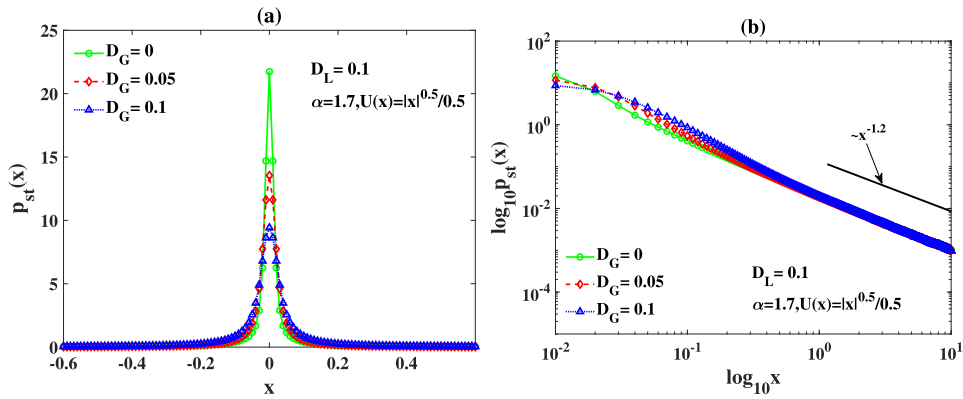
Figure 16. Stationary PDFs for $U(x) = |x|^{0.5}/0.5$, $\alpha = 1.7$, and $D_\mathrm{L} = 0.1$.

for the same D_L. Additionally, for $\alpha = 1.0$, panels (c) and (d) show similar tendencies for the PDF for different noise intensities, although the stationary state does not exist.

For those cases in which a stationary state exists the stationary solutions indeed have power-law tails. Figure 16 presents the stationary PDFs on a log–log scale for $U(x) = |x|^{0.5}/0.5$, $\alpha = 1.7$ and $D_\mathrm{L} = 0.1$. Here panel (a) shows that smaller D_G lead to higher amplitudes of the PDF. Panel (b) shows that the tails of the stationary PDF satisfy $p_\mathrm{st}(x) \simeq |x|^{-1.2}$ when $x \to \infty$. The power-law tails of the stationary solutions are again indifferent to the noise intensity D_G.

7. Conclusions

We derived the FFPKE corresponding to an SDE driven by a combination of Gaussian white noise and α-stable Lévy white noise. The FFPKE is solved for different external potentials: $U(x) = 0$, $U(x) = x^2/2$, $U(x) = x^{2m+2}/(2m + 2)$ $(m = 1, 2, \ldots)$, as well as $U(x) = |x|^c/c$ with $0 < c < 2$. Analytical solutions are derived for some special cases and are verified by numerical solutions. The latter are obtained from the underlying SDE by a Monte Carlo scheme, and from the FFPKE through a finite difference scheme. Analytically, we proved that the solutions of the FFPKE have asymptotic power-law tails. These are of the form $p(x, t) \simeq |x|^{-(\alpha+1)}$ at $|x| \to \infty$ for the constant-potential case. Here, as expected, the power-law exponent is the same as the stable index of the driving Lévy stable noise. For the case $U(x) = x^{2m+2}/(2m + 2)$ $(m = 0, 1, 2, \ldots)$, the PDF will always reach a stationary state characterised by the power-law asymptotic $p_\mathrm{st}(x) \simeq |x|^{-(\alpha+2m+1)}$ at $x \to \infty$. In this case the power-law tails become increasingly steeper, such that for $m \geqslant 1$ the stationary solution has a finite variance, as unveiled earlier for the case of pure Lévy motion in superharmonic potentials [25–27]. In the harmonic case the power-law index of the stationary PDF is identical to the stable index of the driving Lévy noise as seen in [21]. Finally, we proved that in subharmonic potentials of the form $U(x) = |x|^c/c$ the process reaches a stationary state when $c > 2 - \alpha$. In this case the stationary PDF has the power-law asymptotic $p_\mathrm{st}(x) \simeq |x|^{-(c+\alpha-1)}$ for $x \to \infty$. In the limit $c = 2$ this result agrees with the asymptotic in an harmonic potential. For $0 < c < 2$ it thus has a power-law exponent $-(c + \alpha - 1) < -1$ such that the PDF always remains normalisable.

Remarkably, in all cases the emerging power-law tails are independent of the additive Gaussian noise. While it seems fully intuitive that the power-law exponent in all cases is dominated

by the extreme events inherent to the Lévy stable noise, it is nevertheless interesting that the tail behaviour remains unaffected by the noise strength D_G of the additive Gaussian noise. If we interpret the source of the Gaussian noise as a detrimental measurement or setup effect, this means that the asymptotic form of the measured distribution is fully stable against this additional noise. Of course, the pre-asymptotic behaviour of the PDF does show effects from the Gaussian noise, and in this regime our numerical modelling approach can be used to gauge the effect. We note that when we do not focus on the PDF of the process but the first-hitting (first-arrival) time encoded in the dynamics [71, 72], the presence of the additional Gaussian noise is beneficial, as it leads to an effective finite size of the target and thus a faster location [44, 53]. Indeed, the probability to find a point target for Lévy search with $0 < \alpha \leqslant 1$ is zero, that is, such a random search dynamics is absolutely unreliable. However, for the combined Lévy–Brownian search the situation is drastically different: adding Gaussian noise to the equation of motion makes such search completely reliable for $\alpha = 1$ (i.e., the probability to find a point target is 1), whereas the probability for $0 < \alpha < 1$ takes on a nonzero value between 0 and 1, which depends on the intensity of the Gaussian noise. This is completely equivalent to the case of pure Lévy search of a finite-size target. Thus, the intensity of the additive Gaussian noise plays a role analogous to that of the target size [44].

Another remark concerns the potential shapes. In this paper we consider the simplest cases of symmetric external potentials. More complicated shapes will doubtlessly induce new features. For instance, it is known that for pure LFs in an anharmonic single-well potential of the form $U(x) = ax^2 + bx^4$ with non-negative constants a and b a unimodal-bimodal transition in the shape of the stationary PDF takes place on increasing the ratio b/a [25]. Similarly, for pure LFs in a symmetric double-well potential the positions of the maxima of the stationary PDF do not coincide with the positions of the minima of the potential well [73]. It would be of interest to investigate the influence of Gaussian noise on these two effects. Even more complex time evolutions and stationary states are expected for odd and asymmetric potentials. The Langevin dynamics for several systems embedded in specific potentials of such kind and disturbed by Lévy noise have been studied in [74–77].

An interesting extension of the present results would be to combine the Markovian dynamics of the combined, white noises with a non-Poissonian waiting time dynamics in a continuous time random walk formulation [15, 78], or to combine the Lévy white noise with a non-Markovian noise, for instance, fractional Gaussian noise [79]. It will also be of interest to generalise the results obtained here for asymmetric Lévy stable distributions [80]. Finally, we note that recently generic examples of Lévy walks have been considered in confining potentials, demonstrating fundamentally different dynamics from LFs [81–83].

Acknowledgments

Appendix A. Numerical methods

In this appendix, the numerical methods used in this paper are introduced. Appendix A.1 introduces the FD used for solving fractional FPK equation. Appendix A.2 shows the Monte Carlo method for the stochastic differential equation with Gaussian and Lévy noise.

A.1. Finite difference method

In the appendix A.1, the FD scheme is presented for the cases $1 < \alpha \leqslant 2$ (the FD for the $0 < \alpha < 1$ case is similar) and $\alpha = 1$.

Case1: $1 < \alpha \leqslant 2$

For fractional FPK equation

$$\frac{\partial}{\partial t} p(x, t) = \frac{\partial}{\partial x} \left(\frac{U'(x)}{m\gamma} p(x, t) \right) + D_L \frac{\partial^\alpha}{\partial |x|^\alpha} p(x, t) + D_G \frac{\partial^2}{\partial x^2} p(x, t), \quad (A.1)$$

the FD is stated as follows. The time domain $[0, T]$ is divided as $t_n = n\Delta t$, $n = 0, 1, \ldots, L$, where $\Delta t = T/L$. And the spatial domain $[x_{\min}, x_{\max}]$ is discretised into N parts, the length of each part is Δx and $x_j = x_{\min} + j\Delta x$, $j = 0, 1, \ldots, N$.

The Riesz space fractional derivative $\partial^\alpha / \partial |x|^\alpha$ is defined as follows [58, 60]

$$\frac{\partial^\alpha}{\partial |x|^\alpha} p(x_j, t_n) = -\frac{D_+^\alpha p(x_j, t_n) + D_-^\alpha p(x_j, t_n)}{2 \cos(\pi\alpha/2)}, \quad (A.2)$$

where

$$D_+^\alpha p(x, t) = \frac{1}{\Gamma(2 - \alpha)} \frac{d^2}{dx^2} \int_{x_{\min}}^{x} \frac{p(\eta, t) d\eta}{(x - \eta)^{\alpha-1}}, \quad (A.3)$$

and

$$D_-^\alpha p(x, t) = \frac{1}{\Gamma(2 - \alpha)} \frac{d^2}{dx^2} \int_{x}^{x_{\max}} \frac{p(\eta, t) d\eta}{(\eta - x)^{\alpha-1}}. \quad (A.4)$$

Then, according to shifted Grünwald–Letnikov estimates [61–63], we express the fractional space fractional operator as

$$D_+^\alpha p(x_j, t_n) = \frac{1}{\Delta x^\alpha} \sum_{k=0}^{N} c_k p_{j+1-k}^n, \quad (A.5)$$

and

$$D_-^\alpha p(x_j, t_n) = \frac{1}{\Delta x^\alpha} \sum_{k=0}^{N} c_k p_{j-1+k}^n, \quad (A.6)$$

where $c_k = (-1)^k \binom{\alpha}{k} = (-1)^k \frac{\Gamma(\alpha+1)}{\Gamma(k+1)\Gamma(\alpha-k+1)}$, and $p(x_j, t_n) = p_j^n$. By using the difference approximation for the first order derivatives, equation (A.1) can be discretised as

$$\frac{p(x_j, t_{n+1}) - p(x_j, t_n)}{\Delta t} = \frac{U''(x_j)}{m\gamma} p(x_j, t_{n+1})$$

$$+ \frac{U'(x_j)}{m\gamma} \frac{p(x_{j-2}, t_{n+1}) - 8p(x_{j-1}, t_{n+1}) + 8p(x_{j+1,t_{n+1}}) - p(x_{j+2}, t_{n+1})}{12\Delta x}$$

$$-\frac{D_{\mathrm{L}}}{2\,\cos(\pi\alpha/2)\Delta x^{\alpha}}\left(\sum_{k=0}^{N}c_k p_{j+1-k}^{n+1}+\sum_{k=0}^{N}c_k p_{j-1+k}^{n+1}\right)$$

$$-\frac{D_{\mathrm{G}}}{12\Delta x^2}\left(p(x_{j-2},t_{n+1})-16p(x_{j-1},t_{n+1})+30p(x_j,t_{n+1})\right.$$

$$\left.-16p(x_{j+1},t_{n+1})+p(x_{j+2},t_{n+1})\right)\tag{A.7}$$

Moving terms of different time t in equation (A.7) to different sides, equation (A.7) becomes

$$p_j^n=\left(-\frac{U'(x_j)}{m\gamma}\varepsilon_1+\varepsilon_2+Mc_3\right)p_{j-2}^{n+1}+\left(\frac{8U'(x_j)}{m\gamma}\varepsilon_1-16\varepsilon_2+Mc_0+Mc_2\right)p_{j-1}^{n+1}$$

$$+\left(1-\frac{U''(x_j)\Delta t}{m\gamma}+30\varepsilon_2+2Mc_1\right)p_j^{n+1}+\left(-\frac{8U'(x_j)}{m\gamma}\varepsilon_1-16\varepsilon_2+Mc_0+Mc_1\right)p_{j+1}^{n+1}$$

$$+\left(\frac{U'(x_j)}{m\gamma}\varepsilon_1+\varepsilon_2+Mc_3\right)p_{j+2}^{n+1}+M\left(\sum_{k=4}^{N}c_k p_{j+1-k}^{n+1}+\sum_{k=4}^{N}c_k p_{j-1+k}^{n+1}\right)\tag{A.8}$$

where $\varepsilon_1=\Delta t/(12\Delta x)$, $\varepsilon_2=\Delta t D_{\mathrm{G}}/(12\Delta x^2)$, $M=D_{\mathrm{L}}\Delta t/[2\cos(\pi\alpha/2)\Delta x^{\alpha}]$. Equation (A.8) can be expressed in a matric form as (A.7) becomes

$$[T]\{p\}^{n+1}=\{p\}^n,\tag{A.9}$$

where $\{p\}=[p_1,p_2,\ldots p_{N-1}]^T$ and

$$T_{ij}=\begin{cases}1-\dfrac{U''(x_j)\Delta t}{m\gamma}+30\varepsilon_2+2Mc_1, & i=j\\[2mm]-\dfrac{U'(x_j)}{m\gamma}\varepsilon_1+\varepsilon_2+Mc_3, & j=i-2\\[2mm]\dfrac{8U'(x_j)}{m\gamma}\varepsilon_1-16\varepsilon_2+Mc_0+Mc_2, & j=i-1\\[2mm]-\dfrac{8U'(x_j)}{m\gamma}\varepsilon_1-16\varepsilon_2+Mc_0+Mc_1, & j=i+1\\[2mm]\dfrac{U'(x_j)}{m\gamma}\varepsilon_1+\varepsilon_2+Mc_3, & j=i+2\\[2mm]Mc_{i-j+1}, & j\leqslant i-3\\[2mm]Mc_{j-i+1}, & j\geqslant i+3\end{cases}\tag{A.10}$$

where $i,j=1,2,\ldots,N-1$. And we consider the natural boundary condition $p_0=p_N=0$. Besides, the sum of the PDF at each time satisfies the normalisation condition $\sum_{k=0}^{N}p_k=1/\Delta x$.

Case2: $\alpha=1$

$$\frac{\partial}{\partial t}p(x,t)=\frac{\partial}{\partial x}\left(\frac{U'(x)}{m\gamma}p(x,t)\right)+D_{\mathrm{L}}\frac{\partial}{\partial|x|}p(x,t)+D_{\mathrm{G}}\frac{\partial^2}{\partial x^2}p(x,t),\tag{A.11}$$

The time division and space division are the same as case1. But the fractional derivative $\frac{\partial}{\partial|x|}p(x_j, t_n)$ is divided as [57]

$$\frac{\partial}{\partial|x|}p(x_j, t_n) = \frac{1}{\pi\Delta x}\sum_{k=1}^{N}\frac{p(x_{j+k}, t_n) - 2p(x_j, t_n) + p(x_{j-k}, t_n)}{k(k+1)}. \tag{A.12}$$

Following the derivation processes like case 1, a similar iteration in matrix form can be derived as $[T]\{p\}^{n+1} = \{p\}^n$, with $\{p\} = [p_1, p_2, \ldots p_{N-1}]^T$ and

$$T_{ij} = \begin{cases} 1 - \dfrac{U''(x_j)\Delta t}{m\gamma} + 2M\left(1 - \dfrac{1}{N+1}\right) + 30\varepsilon_2, & i = j \\[2mm] -\dfrac{U'(x_j)}{m\gamma}\varepsilon_1 - \dfrac{M}{6} + \varepsilon_2, & j = i - 2 \\[2mm] \dfrac{U'(x_j)}{m\gamma}\varepsilon_1 - \dfrac{M}{6} + \varepsilon_2, & j = i + 2 \\[2mm] 8\dfrac{U'(x_j)}{m\gamma}\varepsilon_1 - \dfrac{M}{2} - 16\varepsilon_2, & j = i - 1, \\[2mm] -8\dfrac{U'(x_j)}{m\gamma}\varepsilon_1 - \dfrac{M}{2} - 16\varepsilon_2, & j = i + 1 \\[2mm] -\dfrac{M}{(i-j)(i-j+1)}, & j \leqslant i - 3 \\[2mm] -\dfrac{M}{(j-i)(j-i+1)}, & j \geqslant i + 3 \end{cases} \tag{A.13}$$

where $i, j = 1, 2, \ldots, N - 1$ and $\varepsilon_1 = \Delta t/(12\Delta x)$, $\varepsilon_2 = \Delta t D_G/(12\Delta x^2)$, $M = D_L\Delta t/(\pi\Delta x)$. And the normalisation condition $\sum_{k=0}^{N}p_k = 1/\Delta x$ is also satisfied.

A.2. Monte Carlo method

For the SDE (1), the Monte Carlo method is adopted based on the solution of Runge–Kutta algorithm as the following form [56]

$$k_1 = f(x(k\Delta t))$$

$$k_2 = f(x(k\Delta t) + \Delta t \times k_1/2)$$

$$k_3 = f(x(k\Delta t) + \Delta t \times k_2/2)$$

$$k_4 = f(x(k\Delta t) + \Delta t \times k_3)$$

$$x([n+1]\Delta t) = x(n\Delta t) + \Delta t \times (k_1 + 2k_2 + 2k_3 + k_4)/6 + \Delta t^{1/\alpha}\xi_n + \Delta t^{1/2}\omega_n. \tag{A.14}$$

Here, ξ_n is Lévy distributed random variables with noise intensity D_L and stability index α. And ω_n is random variables with zero mean and variance $2D_G$. In the above Δt is time step used for iteration. The trajectory of the sample path $x(t)$ is obtained through the Runge–Kutta method. And we carry out the Monte Carlo experiment experiment for 50 000 times and obtain the solution by counting the number of the points in each parts of the interval Δx of the real line x.

ORCID iDs

Yong Xu ⓘ https://orcid.org/0000-0002-8407-4650

Jürgen Kurths ⬤ https://orcid.org/0000-0002-5926-4276
Ralf Metzler ⬤ https://orcid.org/0000-0002-6013-7020

References

[1] Langevin P 1908 Sur la théorie de mouvement brownien *C. R. Hebd. Seances Acad. Sci.* **146** 530

[2] Risken H 1996 *The Fokker–Planck Equation: Methods of Solution and Applications* (Berlin: Springer)

[3] Fogedby H C and Metzler R 2007 DNA bubble dynamics as a quantum Coulomb problem *Phys. Rev. Lett.* **98** 070601

[4] Sun J Q 2006 *Stochastic Dynamics and Control* (Amsterdam: Elsevier)

[5] Liu Q, Xu Y, Xu C and Kurths J 2018 The sliding mode control for an airfoil system driven by harmonic and colored Gaussian noise excitations *Appl. Math. Model.* **64** 249

[6] Mandelbrot B B 1982 *The Fractal Geometry of Nature* (New York: Freeman)

[7] Shlesinger M F and Klafter J 1986 *On Growth and Form* ed H E Stanley (Dordrecht: Kluwer Academic Publishers Group) pp 279–83

[8] Bouchaud J P and Georges A 1990 Anomalous diffusion in disordered media: statistical mechanisms, models and physical applications *Phys. Rep.* **195** 127

[9] Viswanathan G M, da Luz M G E, Raposo E P and Stanley H E 2011 *The Physics of Foraging* (Cambridge: Cambridge University Press)

[10] Xu Y, Duan J Q and Xu W 2011 An averaging principle for stochastic dynamical systems with Lévy noise *Physica* D **240** 1395

[11] Fogedby H C 1994 Langevin equations for continuous time Lévy flights *Phys. Rev.* E **50** 1657

[12] Zaslavsky G M 2002 Chaos, fractional kinetics, and anomalous transport *Phys. Rep.* **371** 461

[13] Compte A 1996 Stochastic foundations of fractional dynamics *Phys. Rev.* E **53** 4191

[14] Metzler R, Barkai E and Klafter J 1999 Deriving fractional Fokker–Planck equations from a generalised master equation *Europhys. Lett.* **46** 431

[15] Metzler R and Klafter J 2000 The random walk's guide to anomalous diffusion: a fractional dynamics approach *Phys. Rep.* **339** 1

[16] Metzler R and Klafter J 2004 The restaurant at the end of the random walk: recent developments in fractional dynamics descriptions of anomalous dynamical processes *J. Phys. A: Math. Gen.* **37** R161

[17] Yanovsky V V, Chechkin A V, Schertzer D and Tur A V 2000 Lévy anomalous diffusion and fractional Fokker–Planck equation *Physica* A **282** 13

[18] Chechkin A V, Tur A V, Schertzer D and Yanovsky V V 1995 Generalized Fokker–Planck equation for anomalous diffusion *Ukrainian J. Phys.* **40** 434

[19] Dubkov A and Spagnolo B 2005 Generalized Wiener process and Kolmogorov's equation for diffusion induced bynon-Gaussian noise source *Fluctuation Noise Lett.* **5** L267

[20] Del-Castillo-Negrete D, Carreras B A and Lynch V E 2004 Fractional diffusion in plasma turbulence *Phys. Plasmas* **11** 3854

[21] Jespersen S, Metzler R and Fogedby H C 1999 Lévy flights in external force fields: Langevin and fractional Fokker–Planck equations and their solutions *Phys. Rev.* E **59** 2736

[22] Chechkin A V and Gonchar V Y 2000 Linear relaxation processes governed by fractional symmetric kinetic equations *J. Exp. Theor. Phys.* **91** 635

[23] Benson D A, Wheatcraft S W and Meerschaert M M 2000 The fractional-order governing equation of Lévy motion *Water Resour. Res.* **36** 1413

[24] Schertzer D, Larchevêque M, Duan J, Yanovsky V V and Lovejoy S 2001 Fractional Fokker–Planck equation for nonlinear stochastic differential equations driven by non-Gaussian Lévy stable noises *J. Math. Phys.* **42** 200

[25] Chechkin A V, Gonchar V Y, Klafter J, Metzler R and Tanatarov L V 2002 Stationary states of non-linear oscillators driven by Lévy noise *Chem. Phys.* **284** 233

[26] Chechkin A V, Klafter J, Gonchar V Y, Metzler R and Tanatarov L V 2003 Bifurcation, bimodality, and finite variance in confined Lévy flights *Phys. Rev.* E **67** 010102

[27] Chechkin A V, Gonchar V Y, Klafter J, Metzler R and Tanatarov L V 2004 Lévy flights in a steep potential well *J. Stat. Phys.* **115** 1505

J. Phys. A: Math. Theor. **53** (2020) 385001

W Zan *et al*

[28] Chechkin A V, Gonchar V Y, Klafter J and Metzler R 2005 Natural cutoff in Lévy flights caused by dissipative non-linearity *Phys. Rev.* E **72** 010101(R)

[29] Gonchar V Y, Tanatarov L V and Chechkin A V 2002 Stationary solutions of the fractional kinetic equation with a symmetric power-law potential *Theor. Math. Phys.* **131** 582

[30] Dubkov A A and Spagnolo B 2007 Langevin approach to Lévy flights in fixed potentials: exact results for stationary probability distributions *Acta Phys. Pol.* B **38** 1745 (www.actaphys.uj.edu.pl/R/38/5/1745/pdf)

[31] Dubkov A A, Spagnolo B and Uchaikin V V 2008 Lévy flight superdiffusion: an introduction *Intern. J. Bifurcation Chaos* **18** 2649

[32] Li Y G, Xu Y and Kurths J 2019 First-passage-time distribution in a moving parabolic potential with spatial roughness *Phys. Rev.* E **99** 052203

[33] Wang Z Q, Xu Y and Yang H 2016 Lévy noise induced stochastic resonance in an FHN model *Sci. China* **59** 371

[34] Li Y G, Mei R X, Xu Y, Kurths J, Duan J Q and Metzler R 2020 Particle dynamics and transport enhancement in a confined channel with position-dependent diffusivity *New J. Phys.* **22** 053016

[35] Ma J Z, Xu Y, Xu W, Li Y G and Kurths J 2019 Slowing down critical transitions via Gaussian white noise and periodic force *Sci. China* **62** 2144

[36] Li Y G, Xu Y, Kurths J and Duan J Q 2019 The influences of correlated spatially random perturbations on first passage time in a linear-cubic potential *Chaos* **29** 101102

[37] Xu Y, Zan W R, Jia W T and Kurths J 2019 Path integral solutions of the governing equation of SDEs excited by Lévy white noise *J. Comput. Phys.* **394** 41

[38] Xu Y, Li Y G, Zhang H, Li X F and Kurths J 2016 The switch in a genetic toggle system with Lévy noise *Sci. Rep.* **6** 31505

[39] Elowitz M B, Levine A J, Siggia E D and Swain P S 2002 Stochastic gene expression in a single cell *Science* **297** 1183

[40] Swain P S, Elowitz M B and Siggia E D 2002 Intrinsic and extrinsic contributions to stochasticity in gene expression *Proc. Natl Acad. Sci. USA* **99** 12795

[41] Lei J Z 2009 Stochasticity in single gene expression with both intrinsic noise and fluctuation in kinetic parameters *J. Theor. Biol.* **256** 485

[42] Pulkkinen O and Metzler R 2013 Distance matters: the impact of gene proximity in bacterial gene regulation *Phys. Rev. Lett.* **110** 198101

[43] Lomholt M A, Ambjörnsson T and Metzler R 2005 Optimal target search on a fast folding polymer chain with volume exchange *Phys. Rev. Lett.* **95** 260603

[44] Palyulin V V, Chechkin A V, Klages R and Metzler R 2016 Search reliability and search efficiency of combined Lévy–Brownian motion: long relocations mingled with thorough local exploration *J. Phys. A: Math. Theor.* **49** 394002

[45] Ditlevsen P D 1999 Observation of α-stable noise induced millennial climate changes from an ice-core record *Geophys. Res. Lett.* **26** 1441

[46] Augello G, Valenti D and Spagnolo B 2010 Non-Gaussian noise effects in the dynamics of a short overdamped Josephson junction *Eur. Phys. J.* B **78** 225

[47] Jeon J H, Barkai E and Metzler R 2013 Noisy continuous time random walks *J. Chem. Phys.* **139** 121916

[48] Viswanathan G M, Afanasyev V, Buldyrev S V, Murphy E J, Prince P A and Stanley H E 1996 Lévy flight search patterns of wandering albatrosses *Nature* **381** 413

[49] Viswanathan G M, Buldyrev S V, Havlin S, da Luz M G, Raposo E P and Stanley H E 1999 Optimizing the success of random searches *Nature* **401** 911

[50] Lomholt M A, Koren T, Metzler R and Klafter J 2008 Lévy strategies in intermittent search processes are advantageous *Proc. Natl Acad. Sci. USA* **105** 11055

[51] Palyulin V V, Chechkin A V and Metzler R 2014 Lévy flights do not always optimize random blind search for sparse targets *Proc. Natl Acad. Sci. USA* **111** 2931

[52] Palyulin V V, Checkin A V and Metzler R 2014 Space fractional Fokker Planck equation and optimization of random search processes in the presence of an external bias *J. Stat. Mech.* P11031

[53] Palyulin V V, Blackburn G, Lomholt M A, Watkins N, Metzler R, Klages R and Chechkin A V 2019 First passage and first hitting times of Lévy flights and Lévy walks *New J. Phys.* **21** 103028

[54] Duan J Q 2015 *An Introduction to Stochastic Dynamics* (Cambridge UK: Cambridge University Press)

[55] Dybiec B, Sokolov I M and Chechkin A V 2010 Stationary states in single-well potentials under symmetric Lévy noises *J. Stat. Mech.* p07008

[56] Honeycutt R L 1992 Stochastic Runge–Kutta algorithms. I. White noise *Phys. Rev.* A **45** 600

[57] Gorenflo R, Mainardi F, Moretti D, Pagnini G and Paradisi P 2002 Discrete random walk models for space-time fractional diffusion *Chem. Phys.* **284** 521

[58] Podlubny I 1998 *Fractional Differential Equations: An Introduction to Fractional Derivatives, Fractional Differential Equations, to Methods of Their Solution and Some of Their Applications* (Amsterdam: Elsevier)

[59] Redner S 2001 *A Guide to First-Passage Processes* (Cambridge UK: Cambridge University Press)

[60] Zeng L and Xu B 2010 Effects of asymmetric Lévy noise in parameter-induced aperiodic stochastic resonance *Physica* A **389** 5128

[61] Liu F, Anh V and Turner I 2004 Numerical solution of the space fractional Fokker–Planck equation *J. Comput. Appl. Math.* **166** 209

[62] Meerschaert M M and Tadjeran C 2006 Finite difference approximations for two-sided space-fractional partial differential equations *Appl. Numer. Math.* **56** 80

[63] Meerschaert M M and Tadjeran C 2004 Finite difference approximations for fractional advection-dispersion flow equations *J. Comput. Appl. Math.* **172** 65

[64] Schneider W R 1986 *Stochastic Processes in Classical and Quantum Systems* (Lecture Notes in Physics, vol 262) ed S Albeverio *et al* (Berlin: Springer)

[65] Mathai A M, Saxena R K and Haubold H J 2010 *The H-Function: Theory and Applications* (New York: Springer)

[66] Chechkin A V, Gorenflo R and Sokolov I M 2002 Retarding subdiffusion and accelerating superdiffusion governed by distributed order fractional diffusion equations *Phys. Rev.* E **66** 046129

[67] Sokolov I M, Chechkin A V and Klafter J 2004 Distributed order fractional kinetics *Acta Phys. Pol.* B **35** 1323 (www.actaphys.uj.edu.pl/R/35/4/1323/pdf)

[68] Chechkin A V, VYu G, Gorenflo R, Korabel N and Sokolov I M 2008 Generalized fractional diffusion equations for accelerating subdiffusion and truncated Lévy flights *Phys. Rev.* E **78** 021111

[69] Sandev T, Chechkin A, Korabel N, Kantz H, Sokolov I M and Metzler R 2015 Distributed-order diffusion equations and multifractality: models and solutions *Phys. Rev.* E **92** 042117

[70] Sandev T, Sokolov I M, Metzler R and Chechkin A 2017 Beyond monofractional kinetics *Chaos Solitons Fractals* **102** 210

[71] Chechkin A V, Metzler R, Klafter J, Gonchar V Y and Tanatarov L V 2003 First passage time density for Lévy flight processes and the failure of the method of images *J. Phys. A: Math. Gen.* **36** L537

[72] Koren T, Lomholt M A, Chechkin A V, Klafter J and Metzler R 2007 Leapover lengths and first passage time statistics for Lévy flights *Phys. Rev. Lett.* **99** 160602

[73] OYu S, Surkov D A, VYu G and Chechkin A V 2013 Stationary states in bistable system driven by Lévy noise *Eur. Phys. J. Spec. Top.* **216** 133

[74] Dubkov A A and Spagnolo B 2008 Verhulst model with Lévy white noise excitation *Eur. Phys. J.* B **65** 361

[75] Dubkov A A, La Cognata A and Spagnolo B 2009 The problem of analytical calculation of barrier crossing characteristics for Lévy flights *J. Stat. Mech.* P01002

[76] Spagnolo B, Valenti D, Guarcello C, Carollo A, Adorno D P, Spezia S, Pizzolato N and Di Paola B 2015 Noise-induced effects in nonlinear relaxation of condensed matter systems *Chaos Solitons Fractals* **81** 412

[77] Spagnolo B, Guarcello C, Magazzú L, Carollo A, Persano Adorno D and Valenti D 2017 Nonlinear relaxation phenomena in metastable condensed matter systems *Entropy* **519** 20

[78] Klafter J, Blumen A and Shlesinger M F 1987 Stochastic pathway to anomalous diffusion *Phys. Rev.* A **35** 3081

[79] Mandelbrot B B and van Ness J W 1968 Fractional Brownian motions, fractional noises and applications *SIAM Rev.* **10** 422

[80] Padash A, Chechkin A V, Dybiec B, Pavlyukevich I, Shokri B and Metzler R 2019 First passage properties of asymmetric Lévy flights *J. Phys. A: Math. Theor.* **52** 454004

[81] Dybiec B, Capala K, Chechkin A V and Metzler R 2019 Conservative random walks in confining potentials *J. Phys. A: Math. Theor.* **52** 015001

[82] Xu P, Zhou T, Metzler R and Deng W 2020 Lévy walk dynamics in an external harmonic potential *Phys. Rev.* E accepted (arXiv:2004.09775)

[83] Dechant A, Kessler D and Barkai E 2015 Deviations from Boltzmann-Gibbs statistics in confined optical lattices *Phys. Rev. Lett.* **115** 173006